

# **Resource Allocation in Collocated Massive MIMO for 5G and Beyond**

Maryam Miriestahbanati

A Thesis

In the Department

of

Electrical and Computer Engineering

Presented in Partial Fulfillment of the Requirements  
For the Degree of  
Master of Applied Science (Electrical Engineering) at  
Concordia University  
Montreal, Quebec, Canada

August 2021

© Maryam Miriestahbanati, 2021

**CONCORDIA UNIVERSITY**  
**SCHOOL OF GRADUATE STUDIES**

This is to certify that the thesis prepared

By: Maryam Miriestahbanati

Entitled: Resource Allocation in Collocated Massive MIMO for 5G and Beyond

and submitted in partial fulfillment of the requirements for the degree of

**Master of Applied Science**

**Electrical Engineering**

complies with the regulations of the University and meets the accepted standards with respect to originality and quality.

Signed by the final examining committee:

Dr. Walaa Hamouda Chair

Dr. Hovhannes Harutyunyan External to Program

Dr. Walaa Hamouda Examiner

Dr. M. Reza Soleymani Thesis Supervisor

Approved by

Dr. Yousef R. Shayan  
Chair of Department or Graduate Program Director

2021-08-25  
Date of Defense

Dr. Mourad Debbabi  
Dean, Gina Cody School of Engineering and Computer Science

## ABSTRACT

### Resource Allocation in Collocated Massive MIMO for 5G and Beyond

Maryam Miriestahbanati

Massive multiuser multiple-input multiple-output (MIMO) systems have been recently introduced as a promising technology for the next generation of wireless networks. It has been proven that linear precoders/detectors such as maximum ratio transmitting/maximum ratio combining (MRT/MRC), zero forcing (ZF), and linear minimum mean square error (LMMSE) on the downlink (DL)/uplink (UL) transmission can provide near optimal performance in such systems.

Acquiring channel state information (CSI) at the transmitter as well as the receiver is one of the challenges in multiuser massive MIMO that can affect the network performance. Any data transmission in multiuser massive MIMO systems starts with the user transmitting UL pilots. The base station (BS) then uses the MMSE estimation method to accurately estimate the CSI from the pilot sequences. Since the UL and DL channels are reciprocal in time division duplex (TDD) mode, the BS employs the obtained CSI to precode the data symbols prior to DL transmission. The users also need the CSI knowledge to accurately decode the DL signals. Beamforming training (BT) scheme is one of the methods that is proposed in the literature to provide the CSI knowledge for the users. In this scheme, the BS precodes and transmits a pilot sequence to the users such that each user can estimate its effective channel coefficients.

Developing an optimal resource distribution method that enhances the system performance is another challenging issue in multiuser massive MIMO. As mentioned earlier, CSI acquisition is one of the requirements of multiuser massive MIMO, and UL pilot transmission is the common method to achieve that. Conventionally, equal powers have been considered for the pilot transmission phase and data transmission phase. However, it can be shown that the performance of the system under this method of power distribution is not optimal.

Therefore, to further improve the performance of multiuser massive MIMO technology, especially in cases where the antenna elements are not well separated and the propagational dispersion is low, optimal resource allocation is required. Hence, the main objective of this

M.A.Sc. thesis is to develop an optimal resource allocation among pilot and data symbols to maximize the spectral efficiency, assuming different receivers such as MRC, ZF, and LMMSE are employed at the BS. Since the calculation of spectral efficiency using the lower bound on the achievable rate is computationally very intensive, we first obtain closed-form expressions for the achievable UL rate of users, assuming the angular domain in the physical channel model is divided into a finite number of separate directions. An approximate expression for spectral efficiency is then developed using the aforementioned closed-form rates. Finally, we propose a resource allocation scheme in which the pilot power, data power, and training duration are optimally chosen in order to maximize the spectral efficiency in a given total power budget.

Extensive simulations are conducted in MATLAB and the results are presented that illustrate the notable improvement in the achievable spectral efficiency through the proposed power allocation scheme. Moreover, the results show that the performance of the proposed method is much superior when the number of channel directions or the number of antennas at BS increases. Furthermore, while the advantage of the proposed method is more notable in the case of ZF and LMMSE receivers, it still outperforms the equal power allocation method for the MRC receiver in terms of spectral efficiency.

## ACKNOWLEDGMENT

I would like to express my great appreciation to my supportive supervisor *Dr. M. Reza Soleymani* for his valuable and constructive suggestions and training during the planning and development of this research work.

I would also like to thank the members of my committee *Dr. Walaa Hamouda* and *Dr. Hovhannes Harutyunyan*.

I dedicate this dissertation to my amazing husband. This would not have been possible without his support and patience. Also, I would like to convey my appreciation to my parents for their endless love and support throughout my life.

# CONTENTS

<b>List of Figures</b> .....	<b>vii</b>
<b>List of Tables</b> .....	<b>viii</b>
<b>List of Acronyms and Notations</b> .....	<b>ix</b>
<b>Chapter 1: Introduction</b> .....	<b>1</b>
1.1 Thesis Motivation.....	2
1.2 Literature Review .....	3
1.3 Thesis Objectives .....	7
1.4 Thesis Scope and Tasks.....	7
1.5 Thesis Layout .....	8
<b>Chapter 2: Background</b> .....	<b>10</b>
2.1 Point-to-point and Multiuser MIMO.....	10
2.2 Multiuser Massive MIMO.....	12
2.3 MRT/MRC, ZF, LMMSE Precoders/Detectors .....	14
2.4 Concluding Remarks .....	16
<b>Chapter 3: Finite-Dimensional Multiuser Massive MIMO</b> .....	<b>18</b>
3.1 System Model.....	18
3.2 Achievable Uplink Rate of MRC Receiver .....	20
3.3 Achievable Uplink Rate of ZF Receiver .....	21
3.4 Achievable Uplink Rate of LMMSE Receiver .....	22
3.5 Concluding Remarks .....	23
<b>Chapter 4: Proposed Resource Allocation Scheme</b> .....	<b>25</b>
4.1 Spectral Efficiency and Optimal Resource Allocation .....	25
4.2 Simulation Results for Different Receivers .....	30
4.3 Concluding Remarks .....	41
<b>Chapter 5: Conclusions and The Future Direction</b> .....	<b>42</b>
5.1 Conclusions .....	42
5.2 Future Works.....	43
<b>Chapter 6: Appendices</b> .....	<b>45</b>
6.1 Appendix I.....	45
6.2 Appendix II .....	47
6.3 Appendix III .....	48
<b>Chapter 7: References</b> .....	<b>51</b>

## LIST OF FIGURES

Figure 1-1- Massive multiuse MIMO system (dashed arrow represents pilot transmission and solid arrow shows data transmission).....	2
Figure 4-1- Spectral efficiency versus $P_p$ for MRC, ZF, and LMMSE receivers (in this figure, SNR = $-5dB$ , $M = 100$ , and $P = 30$ ).....	32
Figure 4-2- Semi-analytic spectral efficiency as well as approximate spectral efficiency (in this figure, $M = 100$ , $P = 30$ , and $P_u = P_p = \frac{P_t}{T}$ ).....	33
Figure 4-3- Semi-analytic spectral efficiency as well as approximate spectral efficiency (in this figure, $M = 200$ , $P = 30$ , and $P_u = P_p = \frac{P_t}{T}$ ).....	34
Figure 4-4- Spectral efficiency versus the number of BS antennas for different UL training durations (in this figure, SNR = $-5dB$ and $P = 30$ ).....	35
Figure 4-5- Spectral efficiency versus the number of BS antennas for different UL training durations (in this figure, SNR = $5dB$ and $P = 30$ ).....	36
Figure 4-6- Spectral efficiency versus the number of BS antennas with equal power and optimum power allocation (in this figure, SNR = $-5dB$ and $P = 30$ ).....	36
Figure 4-7- Spectral efficiency versus the number of BS antennas with equal power and optimum power allocation (in this figure, SNR = $5dB$ and $P = 30$ ).....	37
Figure 4-8- Spectral efficiency versus the number of directions with equal power and optimum power allocation (in this figure, SNR = $0dB$ and $M = 200$ ).....	37
Figure 4-9- Spectral efficiency versus the number of directions with equal power and optimum power allocation (in this figure, SNR = $10dB$ and $M = 200$ ).....	38
Figure 4-10- Optimal pilot power to data power ratio versus the SNR value (in this figure, $M = 150$ ).....	39
Figure 4-11- CDF of spectral efficiency with and without optimal power allocation (in this figure, SNR = $0dB$ , $P = 40$ and $M = 150$ ).....	40
Figure 4-12- CDF of spectral efficiency with and without optimal power allocation (in this figure, SNR = $10dB$ , $P = 40$ and $M = 150$ ).....	40

## LIST OF TABLES

Table 4-1- Sign table of $F(P_P)$ where $\sum_{j=1}^K \beta_j < (T - K)\beta_k$ .....	30
Table 4-2- Sign table of $F(P_P)$ where $\sum_{j=1}^K \beta_j > (T - K)\beta_k$ .....	30
Table 4-3- Sign table of $F(P_P)$ where $\sum_{j=1}^K \beta_j = (T - K)\beta_k$ .....	30
Table 4-4- System parameters for the simulations .....	31

## LIST OF ACRONYMS AND NOTATIONS

Acronym	Description
AP	Access Point
AWGN	Additive White Gaussian Noise
BS	Base Station
CB	Conjugate Beamforming
CDF	Cumulative Distribution Function
CPU	Central Processing Unit
CSI	Channel State Information
DL	Down Link
FDD	Frequency Division Duplex
IoT	Internet of Things
LMMSE	Linear Minimum Mean Square Error
LTE-A	Long Term Evolution Advanced
MIMO	Multiple-Input Multiple-Output
MMSE	Minimum Mean Square Error
mmWave	millimeter-Wave
MRC	Maximum Ratio Combining
MRT	Maximum Ratio Transmitting
OFDM	Orthogonal Frequency Division Multiplexing
SINR	Signal to Interference plus Noise Ratio
SNR	Signal to Noise Ratio
sum-MSE	Sum-Mean Square Error
TDD	Time Division Duplex
UDN	Ultra Dense Network
ZF	Zero Forcing

Symbol	Description
$x^T$	Transpose of $x$
$x^*$	Conjugate of $x$
$x^H$	Conjugate transpose of $x$
$A$	Detector matrix
$C$	Capacity
$D$	Large-scale fading coefficient matrix
$D_v$	Diagonal matrix
$\mathbb{E}\{.\}$	Expected value operator
$G$	Propagation channel matrix
$H$	Small-scale fading coefficient matrix
$\hat{H}$	Estimate of $H$
$I_k$	$k \times k$ identity matrix
$K$	Number of users
$L$	Channel matrix

$M$	Number of antennas at BS
$P$	Number of directions
$P_p$	Pilot power
$P_u$	Data power
$P_t$	Total power
$R$	Achievable rate
$\tilde{R}$	Approximate achievable rate
$SE$	Spectral efficiency
$T$	Channel coherence interval
$\mathbf{u}(\phi_p)$	Steering vector
$\mathbf{U}$	Steering matrix
$\beta$	Large-scale fading coefficient
$\boldsymbol{\varepsilon}$	Channel estimation error matrix
$\tau$	UL training duration

---

## Chapter 1: INTRODUCTION

Due to the rapid evolution of communication technologies and computers, the life cycle of each new generation of the cellular network is approximately a decade or less. The primary issue with the ongoing wireless networks is that they rely on either increasing bandwidth or densifying the cells to achieve the required throughput. These resources are rare, expensive, and are reaching their saturation point [1]. Therefore, the fifth generation of wireless networks will emerge soon. The requirements set for 5G include 100 times higher connected devices and typical user data in comparison to 4G long term evolution advanced (LTE-A), as well as 10 times lower power consumption, and 5 times less latency [2]–[4]. Three major complementary technologies identified to fulfill these requirements of next generation wireless networks are: i) millimeter-wave (mmWave) spectrum occupancy with the carrier frequency range of 30-300 GHz and high available bandwidth [5]–[8], ii) massive multiple-input multiple-output (MIMO) technique with multiple antenna elements at each base station (BS) [9]–[12], and iii) ultra dense networks (UDNs) with extreme utilization of infrastructure in the network [13]–[16].

Multiuser massive MIMO is one of the enabling technologies for delivering 5G services to mobile users with mmWave. Moreover, due to the multi-user diversity in massive multiuser MIMO, the system performance is generally less sensitive to the propagation environment. This makes the multiuser massive MIMO technology an important part of multiple communication standards such as LTE, 802.11, and 802.16. As it is shown in Figure 1-1, in such systems, a BS with a large number of antenna elements serves a number of users in the same time-frequency slot, results in a huge enhancement in the spatial multiplexing and diversity gain [9]–[12], [17], [18]. Moreover, Massive MIMO has the ability to improve both spectral and energy efficiency—even with simple linear processing such as maximum ratio transmitting/maximum ratio combining (MRT/MRC), zero forcing (ZF), and linear minimum mean square error (LMMSE)—and helps to overcome the path loss of mmWave carrier frequencies [19]–[21].

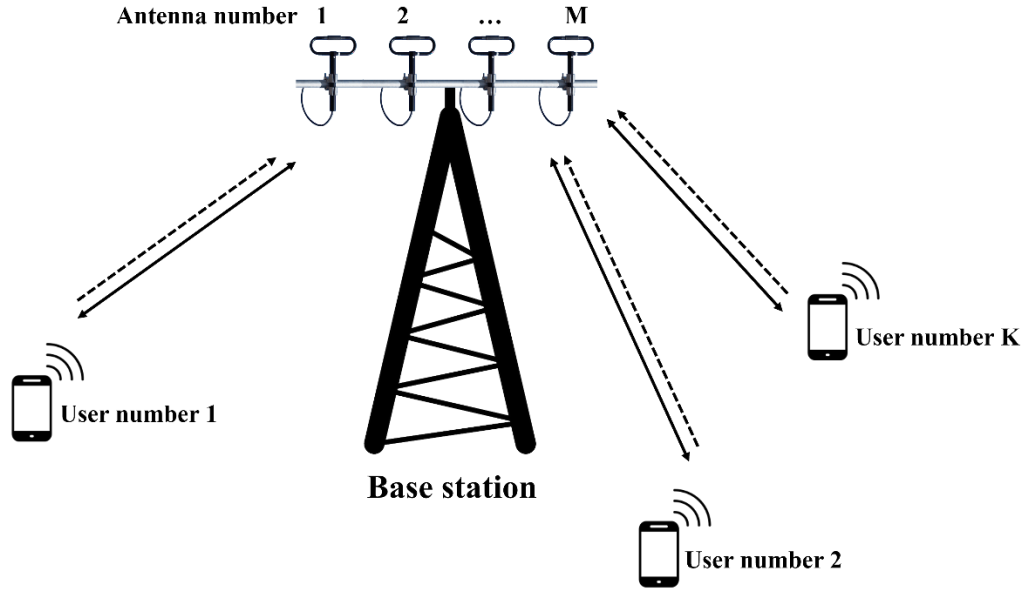


Figure 1-1- Massive multiuser MIMO system (dashed arrow represents pilot transmission and solid arrow shows data transmission)

In this thesis, we consider the situation where the user's channels in massive MIMO are correlated. The reason for this correlation is that the antenna elements are not well separated in practical applications and the propagation dispersion is low [22]. Note that employing optimization methods—in order to enhance spectral efficiency—is crucial in such channels. Hence, by assuming the channel estimation is done through uplink (UL) training, we propose a novel resource allocation in which the data and pilot powers along with the training duration are optimally selected to maximize spectral efficiency.

### 1.1 Thesis Motivation

The growth in the number of mobile devices and smartphones has increased the demand for bandwidth in telecommunication systems. Moreover, the development of various mobile and Internet of Things (IoT) applications has caused a huge surge in need for more bandwidth. The mmWave frequency spectrum with an available large bandwidth can promise a very high rate of data transmission. However, due to the small wavelength of these frequencies, new spatial processing techniques are required. Therefore, we investigate massive MIMO in this thesis, as one of the technologies that enable data transmission through mmWaves. As mentioned before, in practical applications the users' channels in collocated massive MIMO are correlated that results in spectral efficiency degradation [22]–[24]. This motivates us to investigate the UL spectral

efficiency optimization through the resource allocation for such channels, considering multiple receivers such as MRC, ZF, and LMMSE at the BS.

## 1.2 Literature Review

Massive multiuser MIMO systems have recently gained much attention. Its ability to improve the network performance has made it a promising technology for the next generation of wireless networks [9]–[11], [17], [19]–[21], [25], [26]. Specifically, it is shown in [9] that increasing the number of antennas without bound eliminates the effect of intracell interference, fast fading, and uncorrelated noise. It is also indicated in [20] that for  $M \gg K$ , where  $M$  and  $K$  represent the number of antennas at the BS and the number of users respectively, reducing the users' allocated powers in proportion to  $\frac{1}{M}$  for the case of perfect channel state information (CSI) knowledge and to  $\frac{1}{\sqrt{M}}$  for imperfect CSI still results in the same network performance. In addition, massive MIMO systems are employed in the industrial Internet of Things (IoT) to provide connectivity among the devices [27]. Massive MIMO systems can also be used in wireless transmission over Terahertz (THz) bands in order to overcome blockage and mobility [28].

Massive MIMO can be deployed in either a collocated or distributed way. In the collocated case (that is also called cellular massive MIMO and investigated in this thesis), the BS is equipped with a large number of antennas. While in cell-free massive MIMO the antennas are called access points (APs) and distributed randomly all over a coverage area and cover users simultaneously [29]–[34]. In other words, in cell-free massive MIMO users are covered by all or a subset of APs in a user-centric method and therefore, there are no edge users anymore [35]. While spreading the APs over the area increases the backhaul complexity, it improves the coverage probability by using the diversity of shadow fading. Specifically, in [29], it is shown that cell-free massive MIMO improves 95%-likely per user throughput over a small-cell scheme, in which each AP is dedicated to one user. Moreover, a max-min power control algorithm—based on large-scale fading coefficients—is applied in [29], in order to ensure a uniform throughput over the coverage area. In [31], both MRT—called conjugate beamforming (CB) in this paper—and ZF precodings are analyzed in downlink (DL) transmission of a cell-free massive MIMO network. The results emphasize that ZF precoding significantly outperforms MRT precoding. However, ZF cannot be implemented in a distributed way. In other words, all the processing should be done at the CPU, which increases the complexity.

Note that channel hardening and favorable propagation are two main properties of the cellular massive MIMO. Channel hardening means that by scaling up the antenna array in collocated massive MIMO, the channel between the users and antennas at the BS behaves as almost deterministic. In other words, the beamforming in massive MIMO transforms the fading channel into an almost deterministic channel [25]. Favorable propagation is also another property of collocated massive MIMO which means that the channel vectors of the users are almost orthogonal. With this property, the communication performance of users is the same as the situation when the user is alone in the network [36]. In [37], the authors evaluate if the cell-free massive MIMO also inherits the channel hardening and favorable propagation properties. The results in [37] show that for the non-singular path loss model with path loss exponent ( $\alpha$ ) > 2, in order to satisfy the channel hardening condition, the AP density should be  $\lambda_a \sim 1 \text{ AP}/m^2$ , which is an unrealistic condition in practice. In other words, channel hardening is not a valid assumption in deriving the achievable rates of the cell-free massive MIMO for this path loss model. Moreover, the results regarding the investigation of the favorable propagation in cell-free massive MIMO indicate that the higher antenna density, smaller path loss, and larger distance between two users are the factors that help the channels to become nearly orthogonal. Besides, although cell-free massive MIMO is capable of providing more uniform service in the network, it requires more backhauling traffic as well as more infrastructures that increase the network cost [38].

Acquiring the CSI by the BS has a key role in the performance of massive MIMO systems. By using the pilot transmission method followed by MMSE estimation in an UL transmission, the BS accurately estimates the users' channel coefficients and as the result, the transmitted data by users [39]–[41]. Note that since in practical wireless networks the coherence time is not very long, the transmitted pilots in different cells are not typically orthogonal. Hence, to cope with the pilot contamination effect due to this non-orthogonality, various low complex pilot assignment strategies are proposed in [42].

CSI acquisition is also necessary for DL transmission. The BS requires the CSI in order to precode the signals prior to transmission. In frequency division duplex (FDD) operation, the users first estimate the CSI through DL pilots transmitted by the BS and then, send the estimated CSI to the BS over a feedback channel [43]. Note that the number of DL pilots is determined according to the number of antennas at the BS that makes this process very costly. However, according to

the reciprocity property of the channel in the time division duplex (TDD) mode, the BS can apply the estimated CSI in the UL for the DL precoding. In other words, in the TDD mode, the pilot transmission is determined by the number of users. Since in massive MIMO systems, the number of users is less than the antennas at the BS, CSI acquisition under TDD mode is preferable than the FDD mode [44]. The users also need the CSI to decode the transmitted signal in the DL coherently. In some studies, such as [41] and [45], the users are assumed to be aware of the mean of the effective channel gain. While for some practical scenarios in DL transmission that the channel does not harden, the blind estimation method is proposed to improve the DL performance [46].

In most of the studies, orthogonal or independent channel vectors are assumed for users [9], [40], [41]. However, the antenna elements are not well separated in practical applications that results in low propagational dispersion. Therefore, the channel vectors are correlated and can be modeled as  $P$ -dimensional vectors, where  $P$  indicates the number of angular bins [22]–[24], [47]–[49]. Note that in a network with correlated channels and  $M \gg P$ , although the energy efficiency grows in proportion to the number of antennas  $M$ , the throughput gain is no more than that of a network with  $P$  antennas and uncorrelated channels [22]. Besides, it is known that optimal resource allocations can significantly improve the performance. This motivated us to investigate the resource allocation in practical applications with correlated channels, where increasing the number of BS antennas cannot further improve the throughput.

Various resource allocation schemes have been proposed in the literature to further improve the performance of both collocated and cell-free massive multiuser MIMO systems [29], [33], [50]–[58]. Specifically, in [29], by using max-min power control in both the DL and UL of cell-free massive MIMO, the minimum of the rates of all users is maximized. Applying a bisection search to solve this max-min problem results in uniformly good service for all users in different locations. In [33], the total energy efficiency of the cell-free massive MIMO, which is defined as the total throughput divided by the total power consumption (considering both hardware power consumption and backhaul power consumption), is optimized. This energy efficiency maximization is done under the per-antenna power constraint and per-user spectral efficiency constraint. Moreover, in the received-power-based AP selection method proposed in this paper, the selection of APs to serve a user is based on the power control coefficients obtained from the

energy efficiency optimization algorithm. A power allocation scheme among pilot power and data power is proposed in [50] to optimize the sum spectral efficiency of collocated massive MIMO, where only the ZF receiver is investigated at the BS and channel vectors are correlated. By applying a power control technique in [51], the spectral efficiency of collocated massive MIMO is optimized, assuming the peak power of each user is limited, the channel vectors are correlated, and the BS has access to the perfect CSI. In [52], considering only the MRC technique at BS, the authors propose a resource allocation scheme that optimizes the training duration as well as the data and pilot signal powers for uncorrelated users' channel vectors. In [54], a scheduling mechanism for power allocation is investigated in which at any time slot, only a group of users that do not generate interference for each other adjust their power. The authors have proven that applying this mechanism can improve the sum rate per cell in networks with a finite number of BS antennas and a fixed number of users. In [55], for the MRC technique at the BS, a power allocation scheme is proposed in which the power of each pilot symbol and data symbol is optimally selected to maximize spectral efficiency in collocated massive MIMO. In [57], a max-min energy efficiency optimization problem in collocated multiuser massive MIMO is investigated in which the transmit covariance matrix is at first designed per BS and simplified into a beam domain power allocation and then, handled by solving a sequence of convex optimization sub-problems. Also, to solve the sub-problems, two approaches, i.e., a centralized as well as a distributed approach are proposed. In [58], a method of power allocation among pilot and data symbols of all the users is investigated that maximizes the spectral efficiency in DL transmission. Note that in none of the aforementioned studies, spectral efficiency maximization has been considered for the correlated channels where the three linear receivers, namely, MRC, ZF, and LMMSE are employed. Besides, in none of these works, a closed-form expression for lower bound on achievable rate has been obtained that can reduce the computational complexity.

Inspired by the above discussion, we investigate the spectral efficiency maximization through a resource allocation among pilot and data transmissions, where channel vectors are correlated and the three receivers mentioned above are employed. Hence, in this thesis, we propose a scheme in which the training duration, pilot power, and data power are optimally selected to maximize the UL spectral efficiency of a single-cell multiuser massive MIMO scenario. Besides, since the calculation of spectral efficiency using the lower bound on the achievable rate is computationally very intensive, we obtain closed-form expressions for spectral efficiency.

### 1.3 Thesis Objectives

The demand for high rate data transmission has led to research and development efforts towards the new generation of wireless communication systems. Even though in the next generation of wireless systems a dense implementation of APs and new spectral bands will most likely be used, the need for approaches that maximize the spectrum efficiency in a given band will never vanish. As discussed in the previous section, there are a number of works in the literature that investigate the maximization of spectral efficiency in massive multiuser MIMO systems. However, in none of them, the UL spectral efficiency maximization has been considered for the correlated channels where the three linear receivers, namely, MRC, ZF, and LMMSE are employed. Hence, the main objective of this M.A.Sc. thesis is to investigate and propose a solution for resource allocation, as one of the main challenges in collocated massive MIMO with correlated channels. More specifically, we consider the UL transmission in a practical scenario in which the channel vectors are correlated and propose an optimal resource allocation among data and pilot transmissions, in order to improve the network performance.

### 1.4 Thesis Scope and Tasks

In this thesis, by assuming correlated channel vectors, we investigate the spectral efficiency maximization of collocated massive MIMO through a resource allocation scheme for MRC, ZF, and LMMSE receivers. Although the multi-cell scenario is more practical, the single-cell scenario can also be deployed in some applications such as stadiums and rural wireless broadband access [44]. Hence, we focus on the single-cell scenario and make the following contributions:

- Following the method in [22], we derive the achievable UL ergodic rate of the users assuming LMMSE receiver is employed at the BS, the channel vectors are correlated, and the channel estimation is done through UL pilot transmission. Also, to maintain a consistent notation, the UL ergodic rate of MRC and ZF receivers derived in [22] are re-adjusted for the single-cell scenario.
- We derive closed-form approximate UL ergodic rates for MRC, ZF, and LMMSE receivers, assuming a uniform linear array at the BS. We also show that these approximate rates are very accurate and develop an approximation for spectral efficiency based on these rates.

- We propose a resource allocation method in which the data and pilot powers along with the training duration are optimally selected and maximize the spectral efficiency for the three receivers mentioned above. Moreover, in order to find out the receiver for which the proposed power allocation is more effective, a comparison among different receivers is presented.

To show the effectiveness of the proposed resource allocation method, different simulations are conducted in MATLAB under different physical conditions. In fact, the physical parameters that have been considered in this thesis include the number of users, the number of antennas at the BS, the number of channel directions, different signal to noise ratio (SNR) values, different users' locations, UL training duration, pilot power, and data power. It is worth mentioning that the results related to the ZF receiver are published at the IEEE ICC conference [50]. Besides, the extended results related to MRC, ZF, and LMMSE, as well as a comprehensive comparison among all three receivers are published in Physical Communication/Elsevier journal [59].

## 1.5 Thesis Layout

This report is structured as follows:

In chapter 2, we present the fundamental concepts related to point-to-point MIMO, multiuser MIMO, and multiuser massive MIMO and its benefits. Besides, different linear precoders/receivers such as MRC, ZF, and LMMSE are briefly introduced in this chapter.

In chapter 3, the system model that includes a MIMO channel with finite dimensions is presented. Moreover, the UL transmission that consists of the UL pilot transmission and the data transmission phase is investigated. Besides, the achievable UL data transmission rates of MRC, ZF, and LMMSE receivers are derived in this section. Assuming a uniform linear antenna array at the BS, tight closed-form approximate UL rates are also derived for MRC, ZF, and LMMSE receivers.

The spectral efficiency is developed in chapter 4. This chapter also includes the investigation of the proposed power allocation scheme as well as the detailed proof of the concavity of spectral efficiency. This chapter also provides the numerical results developed in MATLAB.

Finally, chapter 5 concludes the report by summarizing the work accomplished in this thesis and specifies the future direction of the research.

*Notation:* boldface small and big letters stand for vectors and matrices, respectively. The superscripts  $T$ ,  $*$ , and  $H$  denote transpose, conjugate, and conjugate transpose, respectively.  $\mathbf{I}_k$  is a  $k \times k$  identity matrix.  $[\mathbf{X}]_{ij}$  shows the  $(i, j)$ th entry of matrix  $\mathbf{X}$ . Finally,  $\mathbf{N} \sim \mathcal{CN}(\mathbf{0}, \mathbf{C})$  represents a complex Gaussian matrix with zero mean and covariance matrix  $\mathbf{C}$ .

## Chapter 2: BACKGROUND

The goal of this thesis is to establish an optimal resource allocation scheme for multiuser massive MIMO systems. Therefore, it is required to review the background related to point-to-point MIMO, multiuser MIMO, and massive MIMO and the existing precoders/receivers for this technology. Hence, we start this chapter with an overview of point-to-point as well as multiuser MIMO. We then investigate multiuser massive MIMO and its potential advantages. Finally, we describe MRT/MRC, ZF, and LMMSE as three main linear precoders/receivers in multiuser massive MIMO.

### 2.1 Point-to-point and Multiuser MIMO

In this section, we first investigate a point-to-point MIMO transmission and present its achievable rate. Then, we briefly investigate the multiuser MIMO channels. Let's assume a transmitter with  $n_t$  antennas serves one receiver with  $n_r$  antennas. Using OFDM in the network converts a frequency-selective wideband channel into multiple flat-fading narrowband channels [9]. Hence, we assume that the MIMO channel is a narrowband time-invariant channel in which the received signal by the receiver can be represented by

$$\mathbf{y} = \sqrt{P_u} \mathbf{G} \mathbf{x} + \mathbf{n}, \quad (2-1)$$

where  $\mathbf{y}$  is the received vector with the size of  $n_r \times 1$ ,  $\mathbf{x}$  is the  $n_t \times 1$  transmitted vector with  $\mathbb{E}\{|\mathbf{x}|^2\} = 1$ ,  $\mathbf{n}$  is  $n_r \times 1$  receiver's additive white Gaussian noise vector ( $\mathbf{n} \sim \mathcal{CN}(0, \mathbf{I})$ ), and  $P_u$  shows the transmitted power or equivalently, the SNR. Under the assumption of perfect knowledge of CSI  $\mathbf{G}$ , the following capacity can be derived for such channel [60]

$$C = I(\mathbf{x}; \mathbf{y}) = \log_2 \left( \det \left( \mathbf{I}_{n_r} + \frac{P_u}{n_t} \mathbf{G} \mathbf{G}^H \right) \right), \quad (2-2)$$

where  $I(\mathbf{x}; \mathbf{y})$  indicates the mutual information operator. Besides, the singular value decomposition of the propagation channel matrix can be represented by

$$\mathbf{G} = \boldsymbol{\varphi} \mathbf{D}_v \boldsymbol{\psi}^H, \quad (2-3)$$

where  $\boldsymbol{\varphi}$  and  $\boldsymbol{\psi}^H$  are the unitary matrices with size  $n_r \times n_r$  and  $n_t \times n_t$ , respectively and  $\mathbf{D}_v$  is the  $n_r \times n_t$  diagonal matrix that comprises the singular values of  $\mathbf{G}$ . Therefore, the capacity given by (2-2) can be rewritten as

$$C = \sum_{j=1}^{\min(n_t, n_r)} \log_2 \left( 1 + \frac{P_u v_j^2}{n_t} \right), \quad (2-4)$$

where  $v_j$ s represent the singular values of  $\mathbf{G}$ . It can be shown that

$$\log_2 \left( 1 + \frac{P_u \text{Tr}(\mathbf{G}\mathbf{G}^H)}{n_t} \right) \leq C \leq \min(n_t, n_r) \times \log_2 \left( 1 + \frac{P_u \text{Tr}(\mathbf{G}\mathbf{G}^H)}{n_t \min(n_t, n_r)} \right), \quad (2-5)$$

where if we assume  $\text{Tr}(\mathbf{G}\mathbf{G}^H) \approx n_t n_r$  (that corresponds to the propagation coefficient magnitude of one), we can get

$$\log_2(1 + P_u n_r) \leq C \leq \min(n_t, n_r) \times \log_2 \left( 1 + \frac{P_u \max(n_t, n_r)}{n_t} \right). \quad (2-6)$$

It is worth noting that the minimum capacity happens in the case of extreme keyhole propagation conditions (where only one of the singular values of  $\mathbf{G}$  has a non-zero value) and the maximum happens if all the elements of  $\mathbf{G}$  are independent random variables.

On the other hand, in multiuser MIMO, the BS is equipped with  $M$  antennas and serves  $K$  single-terminal users simultaneously. Compared to point-to-point MIMO, the advantages of multiuser MIMO include [40]:

- the terminals can be very simple.
- broadcast MIMO can better handle the transition between line-of-sight conditions and rich scattering propagation conditions.
- while the point-to-point MIMO can fail to deliver high-throughput in line-of-sight conditions, the multiuser MIMO can still provide high-throughput under the same condition, as long as the angular separation of the users is larger than the transmit array's Rayleigh resolution.

It can be shown that under favorable conditions (where the users' channel vectors are asymptotically orthogonal), the sum-capacity of broadcast MIMO is comparable to the point-to-point MIMO capacity. In other words,

$$C = \sum_{k=1}^K \log_2(1 + MP_u d_k), \quad (2-7)$$

where  $d_k$  is the large-scale fading coefficients of users.

A drawback of multiuser MIMO is that the BS must know the CSI. Therefore, when the perfect CSI is not available at the BS, the users transmit UL pilot signals prior to the data transmission that increases the overhead. It is known that channel knowledge acquisition is simpler under the TDD operation. In TDD systems, the DL channel matrix is the transpose of the UL channel matrix [25]. Therefore, the BS can employ the channel knowledge acquired through UL pilots for DL precoding prior to the transmission.

## 2.2 Multiuser Massive MIMO

As mentioned in the previous section, multiuser MIMO has big advantages—such as working with cheap single-antenna terminals and simplified resource allocation—over the point-to-point MIMO. However, considering the equal number of transmitted and received antennas as well as frequency division duplex (FDD) operation in multiuser MIMO, make it an unscalable technology. The idea of implementing an unlimited number of antennas at the BS—that later widely accepted as the massive MIMO technique—was firstly introduced by Thomas Marzetta in [9]. In multiuser massive MIMO, with a large number of low-power antenna elements at each BS, the energy is focused on small space regions that brings a huge improvement in throughput and energy efficiency [11]. In general, the potential benefits that can be exploited from massive MIMO can be summarized as follows:

- 1- spectral efficiency: spatial multiplexing of a large number of users creates more multiplexing gain, more throughput, and therefore, higher spectral efficiency. By serving multiple users in the same time-frequency resource in massive MIMO, the achievable spectral efficiency is ten times more than the conventional MIMO [11], [61].
- 2- capacity and link reliability: it is shown that by increasing the number of antennas, the capacity can increase without bound. Besides, the diversity gain provided by massive MIMO increases the link robustness [18].

- 3- energy efficiency: it is shown in [19] that when the number of antennas at the BS increases without bound, the transmit power can be reduced in proportion to  $\frac{1}{M}$  in the case of perfect CSI, and to  $\frac{1}{\sqrt{M}}$  for imperfect CSI, while keeping the same UL rate.
- 4- in addition to the mentioned benefits, security enhancement, robustness improvement, simplified signal processing, and cost efficiency are other advantages provided by massive MIMO [11], [62], [63].

Operating in TDD mode in massive MIMO brings the reciprocity between UL and DL. Therefore, channel coefficients can be estimated at BSs through UL pilot transmission and be used for precoding in DL transmission. In other words, there is no need for DL pilot transmission by BSs and feeding the estimated DL channels back by users [11]. In general, communication and data transmission in massive MIMO has three phases: a) UL pilot transmission, b) UL data transmission, and c) DL data transmission. In the first phase, each user uses  $\tau$  symbols for UL training. All users in the same cell transmit mutually orthogonal pilot sequences contemporarily, which translates into  $\tau \geq K$ , where  $K$  represents the number of active users in each cell. The pilot sequences can be represented by matrix  $\sqrt{\tau P_p} \Phi$  with size  $\tau \times K$ , where  $P_p$  is the power of each pilot symbol, and due to the orthogonality of the pilot sequences we have,

$$\Phi^H \Phi = \mathbf{I}_K. \quad (2-8)$$

After receiving pilots, each BS uses an estimator such as MMSE estimator to approximate the channel coefficients matrix  $\mathbf{G}$  between  $M$  antennas of BS and  $K$  users. Having found the CSI, the BS uses a linear precoder/detector (which is based on the estimated CSI) to encode/separate users' data in DL/UL. In other words, assuming a single-cell multiuser massive MIMO scenario, the signal received by the BS in the UL can be represented by

$$\mathbf{y}_{BS} = \sqrt{P_u} \mathbf{G} \mathbf{x} + \mathbf{n}, \quad (2-9)$$

where  $\mathbf{G}$  is the  $M \times K$  channel matrix, i.e.,  $[\mathbf{G}]_{mk}$  indicates the channel coefficient between the  $m$ th antenna of BS and the  $k$ th user. Moreover,  $P_u$ ,  $\mathbf{x}$ , and  $\mathbf{n}$  represent the average power used by each user, the  $K \times 1$  transmitted data vector of  $K$  users, and the  $M \times 1$  additive white Gaussian noise vector ( $n_m \sim \mathcal{CN}(0,1)$ ), respectively [19]. If  $\mathbf{A}$  shows the  $K \times M$  CSI dependent linear detection matrix, the BS then multiplies the received signal  $\mathbf{y}_{BS}$  by  $\mathbf{A}$  as follows

$$\mathbf{r}_{BS} = \mathbf{A}\mathbf{y}_{BS}. \quad (2-10)$$

In the DL transmission, using precoding matrix  $\mathbf{A}$ , the BS generates the  $M \times 1$  vector  $\mathbf{s}$ , as the input to its antennas, as follows

$$\mathbf{s} = \mathbf{A}^T \mathbf{q}, \quad (2-11)$$

Where  $\mathbf{q}$  is the  $K \times 1$  symbol vector intended for  $K$  users. Therefore, the  $K \times 1$  vector of signals received by  $K$  users equals

$$\mathbf{y}_u = \sqrt{P_f} \mathbf{G}^T \mathbf{s} + \mathbf{w} = \sqrt{P_f} \mathbf{G}^T \mathbf{A}^T \mathbf{q} + \mathbf{w}, \quad (2-12)$$

Where  $P_f$  is the average power used by the BS for transmission of each user's data, and  $w_k \sim \mathcal{CN}(0,1)$  is the additive white Gaussian noise at each user. Finally, assuming users are aware of the mean of the effective channel information, each user tries to decode its own data. In the following subsection, we investigate MRT/MRC, ZF, and LMMSE as three encoders/detectors that are commonly used in massive MIMO.

### 2.3 MRT/MRC, ZF, LMMSE Precoders/Detectors

The complexity issue in massive MIMO is still a concern in practical systems [22]. While the large array antennas can be built by simple antenna units, the signal processing should be also simple. In this subsection, we briefly analyze three linear common precoders/detectors in massive MIMO.

#### 2.3.1 MRT precoder/MRC detector

In MRT/MRC, the encoder/detector matrix is defined as the conjugate-transpose of the estimated channel matrix. In other words, if we assume  $\hat{\mathbf{G}}$  is the channel estimation matrix, the encoding/detection matrix equals

$$\mathbf{A} = \hat{\mathbf{G}}^H. \quad (2-13)$$

In [9], using MRT/MRC as the linear precoder/combiner in DL/UL transmission, it is shown that in a multi-cellular network with an infinite number of antennas, the effect of uncorrelated noise and small-scale fading vanish, the spectral efficiency is independent of bandwidth, and the number of covered users and throughput are also independent of the size of the cells. It is worth mentioning that compared to other linear processors, MRT/MRC has the advantage of being able to be implemented in a distributed manner.

### 2.3.2 ZF precoder/detector

In [64], [65], ZF-based linear algorithms are proposed as methods that can approach the capacity of the MIMO broadcast channel, where the transmitter and receivers have multiple antennas. The ZF processor has the ability to suppress interuser interference. Therefore, it has better performance at higher SNRs. In the case of the ZF transmitter/receiver, the detection matrix  $\mathbf{A}$  equals the pseudo-inverse matrix of the conjugate-transposed channel estimation matrix. In other words,

$$\mathbf{A} = (\widehat{\mathbf{G}}(\widehat{\mathbf{G}}^H \widehat{\mathbf{G}})^{-1})^H. \quad (2-14)$$

Different studies have compared the performance of the MRT/MRC to ZF in different scenarios [10], [22], [39]. In [10], it is shown that as the number of transmitting antennas at the BS grows, ZF precoding performs almost like an interference-free system. Moreover, at low SNRs—especially for a smaller number of antennas at BS—the MRT precoder outperforms ZF in terms of sum-rate capacities and at higher SNRs, ZF has a better performance. It is worth mentioning that the MRT encoder approximates the ZF encoder very well when the antenna array is scaled up. In [22], the achievable UL rate of a massive MIMO system with a finite-dimensional channel model is investigated. The results in [22] emphasize that comparing to MRC, ZF has a better performance when the pilot contamination effect is low, and vice versa. Moreover, for a smaller number of angular bins, MRC is preferable, while for a larger number of angular bins, ZF has a better performance.

### 2.3.3 LMMSE-based precoder/detector

In LMMSE detector, the  $k$ th row of the detection matrix can be defined as

$$\mathbf{a}_k = ((\widehat{\mathbf{G}}\widehat{\mathbf{G}}^H + \frac{1}{P_u} \mathbf{cov}(-\sqrt{P_u} \boldsymbol{\varepsilon} \mathbf{x} + \mathbf{n}))^{-1} \widehat{\mathbf{g}}_k)^H, \quad (2-15)$$

where  $\widehat{\mathbf{g}}_k$  is the  $k$ th column of estimated channel matrix  $\widehat{\mathbf{G}}$ ,  $\boldsymbol{\varepsilon}$  is the channel estimation error matrix, and  $\mathbf{cov}(\boldsymbol{\theta})$  represents the covariance matrix of a random vector  $\boldsymbol{\theta}$  [19]. In general, different optimum formulas are proposed for the LMMSE-based precoding matrix [41], [66]. In [66], the optimum precoding matrix, in order to minimize the sum-mean square error (sum-MSE) of a single-cell multiuser MIMO, is introduced as

$$\mathbf{A} = c(\widehat{\mathbf{G}}^H \widehat{\mathbf{G}} + \frac{K}{P_r+1} \mathbf{I} + \frac{K}{P_d} \mathbf{I})^{-1} \widehat{\mathbf{G}}^H, \quad (2-16)$$

where  $c$  is used to ensure the compliance of power constraint,  $P_r$  denotes the normalized pilot power at each user, and  $P_d$  is the normalized transmit power of the BS.

To summarize, in MRC, by neglecting the effect of multiuser interference and considering it as noise, the received SNR of each stream is maximized. However, the ZF detector neglects the effect of noise and maximizes the SINR by inverting the channel matrix and removing the effect of the channel. Therefore, it has a better performance in the interference-limited scenarios. It is worth mentioning that both MRC and ZF detectors may enhance the noise level, especially when the channel coefficients are small. Therefore, in order to take the effect of noise in the equalization, the LMMSE method is proposed. The LMMSE detector takes the noise effect into consideration and by using the knowledge of SNR, reduces the enhanced interference. Therefore, this detector achieves better performance, especially when the noise power is large [18].

## 2.4 Concluding Remarks

All in all, massive MIMO relies on measuring the frequency responses of the propagation channels. This means users (or BSs) should transmit known training signals and the receiver estimates the channel coefficients and utilizes them before the movement of users significantly changes the channel. In other words, it is assumed in massive MIMO that the total transmission time can be divided into multiple coherence intervals and during each coherence interval, pilot signals should be transmitted prior to the data transmission. In fact, using the measured CSI makes the massive MIMO a scalable technology. However, because of the required overhead for the CSI acquisition, the number of users that can be served simultaneously in one cell is limited. Besides, the re-use of the same pilots in different cells makes the pilot-derived estimate of the channels to be contaminated with interference and hence, degrades the massive MIMO performance [1]. Even though in this thesis we focus on the single-cell scenario and do not take the pilot contamination effect into account, by applying our proposed resource allocation scheme in a multi-cell scenario in the future work, the pilot contamination can also be reduced and the spectral efficiency can be further improved.

Besides, in this thesis, we will consider all three above-mentioned receivers at the BS. In the next chapters, we will analytically derive the achievable UL rates of MRC, ZF, and LMMSE detectors. By assuming a uniform linear antenna array at the BS, we also develop closed-form

approximations for the achievable rate as well as the achievable spectral efficiency of these receivers and present a performance comparison among them.

## Chapter 3: FINITE-DIMENSIONAL MULTIUSER MASSIVE MIMO

In this chapter, we first introduce the MIMO channel with finite dimensions [22]. Then, we investigate the UL training as well as the UL data transmission phases and by assuming the MMSE estimation scheme at the BS, derive the achievable UL rate in the finite-dimensional channel model. Finally, we develop the closed-form per-user achievable UL rate for three different linear detectors at the BS: MRC, ZF, and LMMSE. In chapter 4, we will use the bounds that we derive in this chapter to propose a new resource allocation scheme.

### 3.1 System Model

In a single-cell multi-user massive MIMO, a BS equipped with  $M$  antennas serves  $K$  single-antenna users. We assume the same time-frequency resource is dedicated to all users for UL transmission. Therefore, the  $M \times 1$  received vector at the BS equals

$$\mathbf{y} = \sqrt{P_u} \mathbf{L} \mathbf{x} + \mathbf{n}, \quad (3-1)$$

where  $\mathbf{L}$  is the  $M \times K$  channel matrix between the  $K$  users and  $M$  antennas. Here, we assume the channel is finite-dimensional and therefore, the angular domain provided by the physical channel contains a limited number of directions  $P$ , where  $P \leq M$ . For each direction  $\phi_p$ ,  $p = 1, 2, \dots, P$ , the  $M \times 1$  array steering vector can be written as

$$\mathbf{u}(\phi_p) = \frac{1}{\sqrt{P}} [e^{-jf_1(\phi_p)}, e^{-jf_2(\phi_p)}, \dots, e^{-jf_M(\phi_p)}]^T, \quad (3-2)$$

where  $\phi_p \in [-\pi/2, \pi/2]$ , and  $f_m(\phi)$  is a function of  $\phi$ . Considering a uniform linear antenna array at the BS, (3-2) can be modified to

$$\mathbf{u}(\phi_p) = \frac{1}{\sqrt{P}} \left[ 1, e^{-j2\pi \frac{d}{\lambda} \sin(\phi_p)}, \dots, e^{-j2\pi \frac{(M-1)d}{\lambda} \sin(\phi_p)} \right]^T. \quad (3-3)$$

Let  $g_{pk}$  denote the propagation coefficient of user  $k$  associated with direction  $p$ . Therefore, the channel coefficient between  $k$ th user and the  $m$ th antenna of BS is equal to  $[\mathbf{L}]_{mk} = \sum_{p=1}^P u_m(\phi_p) g_{pk}$ , where  $u_m(\phi_p)$  is the  $m$ th entry of  $\mathbf{u}(\phi_p)$  vector. Hence, the channel matrix between the BS and  $K$  users can be written as

$$\mathbf{L} = \mathbf{U} \mathbf{G}, \quad (3-4)$$

where  $\mathbf{G}$  is the propagation coefficients matrix with size  $P \times K$  that should be estimated at the BS, and  $\mathbf{U} = [\mathbf{u}(\phi_1), \dots, \mathbf{u}(\phi_P)]$  is a full rank  $M \times P$  matrix. The propagation coefficient  $g_{pk}$  can be defined as

$$g_{pk} = h_{pk}\sqrt{\beta_k}, \quad p = 1, \dots, P, \quad (3-5)$$

where  $h_{pk}$  is the fast fading coefficient, and  $\beta_k$  represents the large-scale fading coefficient including path loss and shadowing. The  $h_{pks}, p = 1, \dots, P, k = 1, \dots, K$  are assumed to be independent random variables with zero-mean and unit variance complex Gaussian distribution, i.e.,  $\mathcal{CN}(0,1)$ .  $\beta_k, k = 1, \dots, K$  are also supposed to be constant over several coherence intervals and known a priori. Therefore, we can represent matrix  $\mathbf{G}$  as

$$\mathbf{G} = \mathbf{H}\mathbf{D}^{1/2}, \quad (3-6)$$

where  $\mathbf{H}$  and  $\mathbf{D}$  are the  $P \times K$  fast fading coefficients matrix and  $K \times K$  diagonal matrix of the large-scale fading coefficients, respectively. Note that the BS needs to estimate the matrix  $\mathbf{H}$ , while  $\mathbf{U}$  and  $\mathbf{D}$  are known. Therefore, UL pilots are employed to provide an estimation of the matrix  $\mathbf{H}$ . We assume each user uses  $\tau \geq K$  symbols for UL training, where pilot sequences are mutually orthogonal and can be represented by matrix  $\sqrt{\tau P_P}\mathbf{\Phi}$ . Therefore, the  $M \times \tau$  received pilot matrix at the BS can be denoted by

$$\mathbf{Y}_p = \sqrt{\tau P_P}\mathbf{L}\mathbf{\Phi}^T + \mathbf{N} = \sqrt{\tau P_P}\mathbf{U}\mathbf{G}\mathbf{\Phi}^T + \mathbf{N}, \quad (3-7)$$

where  $\mathbf{N}$  is  $M \times \tau$  complex AWGN matrix with i.i.d elements with zero mean and variance equals one, i.e.,  $\mathbf{N} \sim \mathcal{CN}(0,1)$ . In order to estimate the channel, the BS projects the received pilot matrix on  $\mathbf{\Phi}^*$ . Therefore, we have

$$\tilde{\mathbf{Y}}_p = \mathbf{Y}_p\mathbf{\Phi}^* = \sqrt{\tau P_P}\mathbf{U}\mathbf{H}\mathbf{D}^{1/2} + \tilde{\mathbf{N}}, \quad (3-8)$$

where  $\tilde{\mathbf{N}} = \mathbf{N}\mathbf{\Phi}^* \sim \mathcal{CN}(\mathbf{0}, \mathbf{I}_{(MK \times MK)})$ . Since the columns of  $\mathbf{H}$  are independent, its  $k$ th column can be estimated independently and according to  $\tilde{\mathbf{y}}_{p,k}$ , that is the  $k$ th column of the projected received pilot matrix. Using the MMSE estimator, we have [67]

$$\hat{\mathbf{h}}_k = \sqrt{\tau P_P\beta_k}(\tau P_P\mathbf{U}^H\beta_k + \mathbf{I}_P)^{-1}\mathbf{U}^H\tilde{\mathbf{y}}_{p,k}, \quad (3-9)$$

where  $\tilde{\mathbf{y}}_{p,k} = \sqrt{\tau P_P}\mathbf{U}\mathbf{h}_k\sqrt{\beta_k} + \tilde{\mathbf{n}}_k$ . By estimating each column of  $\mathbf{H}$ , the estimation of channel matrix  $\mathbf{L}$  can be represented as

$$\hat{\mathbf{L}} = \mathbf{U}\hat{\mathbf{H}}\mathbf{D}^{1/2}. \quad (3-10)$$

The channel estimation error can also be defined as  $\boldsymbol{\varepsilon} = \hat{\mathbf{L}} - \mathbf{L}$ , that according to the MMSE estimation properties, is independent of  $\hat{\mathbf{L}}$ .

As mentioned before, the BS uses a linear detector to separate the received user data streams. Therefore, according to (2-10) we have

$$\mathbf{r} = \sqrt{P_u}\mathbf{A}\mathbf{L}\mathbf{x} + \mathbf{A}\mathbf{n}. \quad (3-11)$$

Let  $r_k$  be the  $k$ th element of the received vector  $\mathbf{r}$  and  $x_k$  be the transmitted signal of the  $k$ th user. In order to obtain the lower bound of the achievable UL rate of this user, we write

$$r_k = \sqrt{P_u}\mathbf{a}_k\hat{\mathbf{l}}_k x_k + \sum_{j=1, j \neq k}^K \sqrt{P_u}\mathbf{a}_k\hat{\mathbf{l}}_j x_j - \sum_{j=1}^K \sqrt{P_u}\mathbf{a}_k\boldsymbol{\varepsilon}_j x_j + \mathbf{a}_k \mathbf{n}. \quad (3-12)$$

Therefore, the following UL rate is achievable for the  $k$ th user in the network.

$$R_k = \mathbb{E}\{\log_2(1 + \text{SINR}_k)\}, \quad (3-13)$$

where

$$\text{SINR}_k = \frac{p_u |\mathbf{a}_k \hat{\mathbf{l}}_k|^2}{\mathbb{E}\{|\sqrt{p_u} \sum_{j=1, j \neq k}^K \mathbf{a}_k \hat{\mathbf{l}}_j x_j|^2 | \mathbf{a}_k, \hat{\mathbf{l}}_k\} + p_u \sum_{j=1}^K \mathbf{a}_k \text{cov}(\boldsymbol{\varepsilon}_j) \mathbf{a}_k^H + \|\mathbf{a}_k\|^2}. \quad (3-14)$$

In the following subsections, we will derive the achievable ergodic rate of the UL transmission from the  $k$ th user to the BS for MRC, ZF, and LMMSE receivers. Then, assuming  $M$  to be large enough, we develop an approximate closed-form formula for the ergodic rates.

### 3.2 Achievable Uplink Rate of MRC Receiver

For the MRC receiver, the first term in the denominator of (3-14) can be given by

$$\mathbb{E}\left\{\left|\sqrt{p_u} \sum_{j=1, j \neq k}^K \mathbf{a}_k \hat{\mathbf{l}}_j x_j\right|^2 | \mathbf{a}_k, \hat{\mathbf{l}}_k\right\} = p_u \hat{\mathbf{l}}_k^H \left( \sum_{j=1, j \neq k}^K \text{cov}(\hat{\mathbf{l}}_j) \right) \hat{\mathbf{l}}_k. \quad (3-15)$$

Accordingly, by substituting (2-13) and (3-15) into (3-14) and using the fact that  $\text{cov}(\hat{\mathbf{l}}_j) = \beta_j \mathbf{U}\mathbf{U}^\dagger - \text{cov}(\boldsymbol{\varepsilon}_j)$ , we have

$$R_k^{\text{MRC}} = \mathbb{E}\left\{\log_2\left(1 + \frac{\|\hat{\mathbf{l}}_k\|^4}{\hat{\mathbf{l}}_k^H [(\sum_{j=1}^K \beta_j) \mathbf{U}\mathbf{U}^H - \text{cov}(\hat{\mathbf{l}}_k)] \hat{\mathbf{l}}_k + \frac{1}{P_u} \|\hat{\mathbf{l}}_k\|^2}\right)\right\}, \quad (3-16)$$

where  $\mathbf{cov}(\hat{\mathbf{l}}_k) = \tau P_p \beta_k^2 \mathbf{U} (\tau P_p \mathbf{U}^H \mathbf{U} \beta_k + \mathbf{I}_P)^{-1} \mathbf{U}^H \mathbf{U} \mathbf{U}^H$ . It can be shown that for a uniform linear antenna array given by (3-3), we have

$$\frac{1}{M} \mathbf{u}^H(\phi_p) \mathbf{u}(\phi_q) = \frac{1}{MP} \sum_{m=0}^{M-1} e^{j2\pi \frac{d}{\lambda} (\sin(\phi_p) - \sin(\phi_q)) m}. \quad (3-17)$$

If  $p = q$ , (3-17) equals  $\frac{1}{P}$ . For  $p \neq q$  and  $M$  large enough, (3-17) can be approximated by

$$\frac{1}{M} \mathbf{u}^H(\phi_p) \mathbf{u}(\phi_q) = \frac{1}{MP} \frac{1 - e^{j2\pi \frac{d}{\lambda} (\sin(\phi_p) - \sin(\phi_q)) M}}{1 - e^{j2\pi \frac{d}{\lambda} (\sin(\phi_p) - \sin(\phi_q))}} \approx 0. \quad (3-18)$$

Hence, when the number of antennas ( $M$ ) is large enough, we have

$$\frac{1}{M} \mathbf{U}^H \mathbf{U} \approx \frac{1}{P} \mathbf{I}_P. \quad (3-19)$$

Using (3-19), a closed-form approximation for the ergodic rate of users can be achieved as follows.

**Theorem 1:** Using MRC processing at the BS, a closed-form approximation for the achievable ergodic rate given by (3-16) can be obtained as

$$\tilde{R}_k^{MRC} = \log_2 \left( 1 + \frac{\frac{\tau P_p \beta_k^2}{M} (P-1) \left(\frac{M}{P}\right)^2}{\tau P_p \frac{M}{P} \beta_k + 1} \right) \left( \frac{\frac{M}{P} (\sum_{j=1}^K \beta_j) - \frac{\tau P_p \beta_k^2}{M} \left(\frac{M}{P}\right)^2 + \frac{1}{P_u}}{\tau P_p \frac{M}{P} \beta_k + 1} \right). \quad (3-20)$$

**Proof:** See appendix I.

### 3.3 Achievable Uplink Rate of ZF Receiver

The detection matrix of a ZF receiver is given by (2-14). Therefore, it can be shown that the achievable UL rate of data transmission from  $k$ th user to the BS with ZF receiver yields to

$$R_k^{ZF} = \mathbb{E} \left\{ \log_2 \left( 1 + \frac{1}{\sum_{j=1}^K [(\hat{\mathbf{L}}^H \hat{\mathbf{L}})^{-1} \hat{\mathbf{L}}^H \mathbf{cov}(\boldsymbol{\varepsilon}_j) \hat{\mathbf{L}} (\hat{\mathbf{L}}^H \hat{\mathbf{L}})^{-1}]_{kk} + \frac{1}{P_u} [(\hat{\mathbf{L}}^H \hat{\mathbf{L}})^{-1}]_{kk}} \right) \right\}, \quad (3-21)$$

where  $\mathbf{cov}(\boldsymbol{\varepsilon}_j)$  represents the covariance matrix of vector  $\boldsymbol{\varepsilon}_j$  that equals

$$\mathbf{cov}(\boldsymbol{\varepsilon}_j) = \beta_j \mathbf{U} \mathbf{U}^H - \tau P_p \beta_j^2 \mathbf{U} (\tau P_p \mathbf{U}^H \mathbf{U} \beta_j + \mathbf{I}_P)^{-1} \mathbf{U}^H \mathbf{U} \mathbf{U}^H. \quad (3-22)$$

Using the approximation given by (3-19), an approximate closed-form achievable UL rate can be derived as follows.

**Theorem 2:** Using ZF receiver at the BS, a closed-form approximation for  $R_k^{ZF}$  given by (3-21) can be obtained as

$$\tilde{R}_k^{ZF} = \log_2 \left( 1 + \frac{\frac{\tau P_P \beta_k^2}{\tau P_P \frac{M}{P} \beta_k + 1} (P - K) \left(\frac{M}{P}\right)^2}{\frac{M}{P} \left( \sum_{j=1}^K \frac{\beta_j}{\tau P_P \frac{M}{P} \beta_j + 1} \right) + \frac{1}{P_u}} \right). \quad (3-23)$$

**Proof:** See appendix II.

### 3.4 Achievable Uplink Rate of LMMSE Receiver

According to (2-15), the  $k$ th column of the detection matrix for the case of LMMSE receiver equals

$$\begin{aligned} \mathbf{a}_k &= \left( (\hat{\mathbf{L}} \hat{\mathbf{L}}^H + \frac{1}{p_u} \mathbf{cov}(-\sqrt{P_u} \boldsymbol{\varepsilon} \mathbf{x} + \mathbf{n}))^{-1} \hat{\mathbf{l}}_k \right)^* \\ &= \frac{\boldsymbol{\Lambda}_k^{-1} \hat{\mathbf{l}}_k}{\hat{\mathbf{l}}_k^H \boldsymbol{\Lambda}_k^{-1} \hat{\mathbf{l}}_k + 1}, \end{aligned} \quad (3-24)$$

where  $\boldsymbol{\Lambda}_k = \sum_{j=1, j \neq k}^K \hat{\mathbf{l}}_j \hat{\mathbf{l}}_j^H + \sum_{j=1}^K \mathbf{cov}(\boldsymbol{\varepsilon}_j) + \frac{1}{P_u} \mathbf{I}_M$ . Similar to the previous receivers, by substituting (3-24) into (3-14), we obtain the following ergodic UL rate.

$$\begin{aligned} R_k^{LMMSE} &= \mathbb{E} \left\{ \log_2 \left( 1 + \hat{\mathbf{l}}_k^H \boldsymbol{\Lambda}_k^{-1} \hat{\mathbf{l}}_k \right) \right\} \\ &= \mathbb{E} \left\{ \log_2 \left( \frac{1}{1 - \hat{\mathbf{l}}_k^\dagger [\sum_{j=1}^K (\hat{\mathbf{l}}_j \hat{\mathbf{l}}_j^H + \mathbf{cov}(\boldsymbol{\varepsilon}_j)) + \frac{1}{P_u} \mathbf{I}_M]^{-1} \hat{\mathbf{l}}_k} \right) \right\} \\ &= \mathbb{E} \left\{ \log_2 \left( \frac{1}{1 - [\hat{\mathbf{L}}^H [\sum_{j=1}^K (\hat{\mathbf{l}}_j \hat{\mathbf{l}}_j^H + \mathbf{cov}(\boldsymbol{\varepsilon}_j)) + \frac{1}{P_u} \mathbf{I}_M]^{-1} \hat{\mathbf{L}}]_{kk}} \right) \right\}, \end{aligned} \quad (3-25)$$

where the second equality is resulted directly from (3-24). Similar to MRC and ZF receivers, by applying the approximation given by (3-19), a closed-form achievable UL ergodic rate can be found using the following theorem.

**Theorem 3:** Considering LMMSE receiver at the BS, the achievable UL ergodic rate can be approximated by the following closed-form expression.

$$\tilde{R}_k^{LMMSE} = \log_2 \left( 1 + \left( \frac{(P - K + 1 + (K - 1)\hat{\mu}_k)^2}{P - K + 1 + (K - 1)\hat{\delta}_k} - 1 \right) \theta_k \right), \quad (3-26)$$

where

$$\theta_k = \frac{P - K + 1 + (K - 1)\hat{\delta}_k}{P - K + 1 + (K - 1)\hat{\mu}_k} \times \hat{\zeta}_{k'},$$

$$\hat{\zeta}_k = \frac{\tau P_p P_u \beta_k^2 \left(\frac{M}{P}\right)^2}{\left(\tau P_p \beta_k \frac{M}{P} + 1\right) \left(1 + P_u \frac{M}{P} \sum_{j=1}^K \frac{\beta_j}{\tau P_p \beta_j \frac{M}{P} + 1}\right)}, \quad (3-27)$$

and  $\hat{\mu}_k$  and  $\hat{\delta}_k$  can be found by solving the following equations

$$\hat{\mu}_k = \frac{1}{K - 1} \sum_{k'=1, k' \neq k}^K \frac{1}{P \hat{\zeta}_{k'} \left(1 - \frac{K - 1}{P} + \frac{K - 1}{P} \hat{\mu}_k\right) + 1},$$

$$\hat{\delta}_k \left(1 + \sum_{k'=1, k' \neq k}^K \frac{\hat{\zeta}_{k'}}{\left(P \hat{\zeta}_{k'} \left(1 - \frac{K - 1}{P} + \frac{K - 1}{P} \hat{\mu}_k\right) + 1\right)^2}\right)$$

$$= \sum_{k'=1, k' \neq k}^K \frac{\hat{\zeta}_{k'} \hat{\mu}_k + \frac{1}{K - 1}}{\left(P \hat{\zeta}_{k'} \left(1 - \frac{K - 1}{P} + \frac{K - 1}{P} \hat{\mu}_k\right) + 1\right)^2}. \quad (3-28)$$

**Proof:** See appendix III.

It is worth mentioning that the approximate rates given by (3-20), (3-23), and (3-26) are very close to the exact UL ergodic rates and approach tight lower bounds as  $M \rightarrow \infty$ .

### 3.5 Concluding Remarks

The finite-dimensional channel model is an interesting system model that takes the non-orthogonality of users' channels into account. In this chapter, by considering this system model, we investigated the achievable UL ergodic rate of MRC, ZF, and LMMSE receivers as the performance metric. Assuming a uniform linear antenna array at the BS, we further developed closed-form approximate expressions for the achievable rates in three distinct theorems, namely Theorem 1, Theorem 2, and Theorem 3. We also proved that these closed-forms are very accurate and approach tight lower bounds. The developed rates in Theorems 1, 2, and 3 showed that the pilot and data transmission powers have a substantial role in the achievable UL rates. Therefore,

in the next chapter, we present a resource allocation scheme that by optimally selecting the pilot and data powers, maximizes the users' UL rates.

## Chapter 4: PROPOSED RESOURCE ALLOCATION SCHEME

In this chapter, we first develop spectral efficiency by employing the approximate achievable rates found in the previous chapter. Then, we prove that the developed spectral efficiency is a concave function with respect to the pilot power/data power. By proposing an optimal resource allocation, we also maximize spectral efficiency, as the performance metric in our analysis. Finally, we present the simulation results that verify the mathematical analysis.

### 4.1 Spectral Efficiency and Optimal Resource Allocation

Let  $T$  indicate the length of coherence interval in symbols. If an interval of  $\tau$  symbols is allocated to the UL training,  $T - \tau$  symbols remain for UL data transmission. Hence, the spectral efficiency can be represented by

$$SE = \frac{T - \tau}{T} \sum_{k=1}^K \tilde{R}_k. \quad (4-1)$$

As mentioned before, pilot and data powers have a substantial role in the achievable UL rate and hence, the spectral efficiency. Therefore, optimal power distribution between the training and UL data transmission along with the optimal length of pilot symbols can improve the spectral efficiency, and accordingly, the system performance. In this view, we propose a resource allocation scheme that optimally selects  $\tau$ ,  $P_p$ , and  $P_u$  in one coherence interval to maximize spectral efficiency. Mathematically speaking, we have

$$\begin{aligned} & \max_{P_p, P_u, \tau} SE \\ & \text{subject to } \begin{cases} \tau P_p + (T - \tau) P_u \leq P_t, \\ K \leq \tau \leq T, (\tau \in \mathbb{N}), \\ P_p \geq 0, P_u \geq 0, \end{cases} \end{aligned} \quad (4-2)$$

where  $P_t$  is the total available power for each user in one coherence interval.

**Proposition 1:** The spectral efficiency given by (4-1) is maximized when the whole allocated power in each coherence interval ( $P_t$ ) is consumed by the users.

**Proof:** By substituting the rates found in the previous chapter into (4-1), it can be shown that the spectral efficiency is an increasing function of  $P_p$  when  $\tau$  and  $P_u$  are given. Besides, for a given  $\tau$  and  $P_p$ , spectral efficiency is an increasing function of  $P_u$ . Hence, spectral efficiency is maximized when each user consumes the whole allocated power. As the result, the first inequality constraint in (4-2) changes to equality. ■

**Lemma 1:** The optimal value of  $\tau$  in the optimization problem given by (4-2) is equal to the number of users  $K$ .

**Proof:** The spectral efficiency can be rewritten as

$$SE(\tau, P_P, P_u) = \sum_{k=1}^K f_k(\tau, P_P, P_u), \quad (4-3)$$

where for MRC receiver

$$f_k(\tau, P_P, P_u) = \left(1 - \frac{\tau}{T}\right) \times \log_2 \left( 1 + \frac{\tau P_P \beta_k^2 (P-1) \left(\frac{M}{P}\right)^2}{v_1 (\sum_{j=1, j \neq k}^K \beta_j) + \frac{M}{P} \beta_k + \left(\tau P_P \frac{M}{P} \beta_k + 1\right) \frac{1}{P_u}} \right), \quad (4-4)$$

for ZF receiver

$$f_k(\tau, P_P, P_u) = \left(1 - \frac{\tau}{T}\right) \times \log_2 \left( 1 + \frac{\tau P_P \beta_k^2 (P-K) \left(\frac{M}{P}\right)^2}{v_1 \left( \sum_{j=1}^K \frac{\beta_j}{\tau P_P \beta_j \frac{M}{P} + 1} \right) + \left(\tau P_P \frac{M}{P} \beta_k + 1\right) \frac{1}{P_u}} \right), \quad (4-5)$$

and for LMMSE receiver

$$f_k(\tau, P_P, P_u) = \left(1 - \frac{\tau}{T}\right) \times \log_2 \left( 1 + v_2 \frac{\tau P_P P_u \beta_k^2 \left(\frac{M}{P}\right)^2}{\left(\tau P_P \frac{M}{P} \beta_k + 1\right) \left( 1 + P_u \frac{M}{P} \sum_{j=1}^K \frac{\beta_j}{\tau P_P \beta_j \frac{M}{P} + 1} \right)} \right), \quad (4-6)$$

and  $v_1 = \left(\tau P_P \beta_k \left(\frac{M}{P}\right)^2 + \frac{M}{P}\right)$  and  $v_2 = \left(P - K + 1 + (K-1) \hat{\mu}_k - \frac{P-K+1+(K-1)\hat{\delta}_k}{P-K+1+(K-1)\hat{\mu}_k}\right)$ . Let  $\tau^*$ ,  $P_P^*$ , and  $P_u^*$  be the optimal solutions of (4-2) that satisfy all the constraints and  $\tau^* > K$ . Let's choose  $\tilde{\tau} =$

$K, \tilde{P}_p = \frac{\tau^* P_p^*}{K}$ , and  $\tilde{P}_u = \frac{P_t - \tau^* P_p^*}{T - \tilde{\tau}}$  that also satisfy the constraints in (4-2). Since  $\tau^* P_p^* = \tilde{\tau} \tilde{P}_p$  and considering the fact that  $g(x) = x \log_2(1 + \frac{a}{b+cx})$  with  $a, b, c > 0$  is a strictly increasing function in  $x \in (0, \infty)$  [55], for MRC, ZF, and LMMSE receivers we can show that

$$f_k(\tilde{\tau}, \tilde{P}_p, \tilde{P}_u) > f_k(\tau^*, P_p^*, P_u^*), \quad (4-7)$$

And hence,

$$SE(\tilde{\tau}, \tilde{P}_p, \tilde{P}_u) > SE(\tau^*, P_p^*, P_u^*), \quad (4-8)$$

that contradicts with the optimality of  $\tau^*, P_p^*$ , and  $P_u^*$  and therefore,  $\tau^* \leq K$ . On the other hand, to have orthogonal pilots, we have  $\tau^* \geq K$ . This implies that the optimum value of  $\tau$  is equal to  $K$ . ■

Therefore, according to Proposition 1 and Lemma 1, the optimization problem given by (4-2) can be simplified to

$$\begin{aligned} & \max_{P_p} SE \\ & \text{subject to} \begin{cases} 0 \leq P_p \leq \frac{P_t}{K}, \\ P_u = \frac{P_t - KP_p}{(T - K)}. \end{cases} \end{aligned} \quad (4-9)$$

**Theorem 4:** The objective function in (4-9) is a concave function with respect to  $P_p$  for MRC, ZF, and LMMSE receivers.

**Proof:** In this thesis, we prove the concavity of (4-9) assuming the MRC receiver is employed at the BS. The concavity of spectral efficiency for ZF and LMMSE receivers can be shown by applying the same method. Considering  $\tau = K$  and  $P_u = \frac{P_t - KP_p}{(T - K)}$ , the  $\text{SINR}_k^{\text{MRC}}$  in (3-20) can be written as

$$\begin{aligned} & \text{SINR}_k^{\text{MRC}} \\ &= \frac{KP_p \beta_k^2 (P - 1) \left(\frac{M}{P}\right)^2}{\underbrace{\left(KP_p \left(\frac{M}{P}\right)^2 \beta_k + \frac{M}{P}\right) \left(\sum_{j=1, j \neq k}^K \beta_j\right) + \frac{M}{P} \beta_k + \left(KP_p \frac{M}{P} \beta_k + 1\right) \frac{T - K}{P_t - KP_p}}_D}. \end{aligned} \quad (4-10)$$

The first derivative of  $\text{SINR}_k^{\text{MRC}}$  with respect to  $P_p$  can be given by

$$\frac{d}{dP_p} (\text{SINR}_k^{\text{MRC}}) = \frac{K \beta_k^2 (P - 1) \left(\frac{M}{P}\right)^2 F(P_p)}{D^2 (P_t - KP_p)^2}, \quad (4-11)$$

where  $F(P_p)$  is a second order polynomial function of  $P_p$  that is equal to

$$\begin{aligned}
F(P_p) &= P_p^2 \left( \frac{M}{P} \left( \sum_{j=1}^K \beta_j \right) K^2 - \frac{M}{P} K^2 (T - K) \beta_k \right) \\
&\quad + P_p \left( -2 \frac{M}{P} \left( \sum_{j=1}^K \beta_j \right) K P_t - 2K(T - K) \right) \\
&\quad + \left( \frac{M}{P} \left( \sum_{j=1}^K \beta_j \right) P_t^2 + (T - K) P_t \right) = AP_p^2 + BP_p + C.
\end{aligned} \tag{4-12}$$

Since  $\frac{K\beta_k^2(P-1)\left(\frac{M}{P}\right)^2}{D^2(P_t-KP_p)^2}$  is positive, the roots as well as the sign table of (4-11) and (4-12) are the same.

Hence, we continue the proof of concavity by finding the roots and the sign table of  $F(P_p)$ . To do so, we consider the three following cases:

1-  $\sum_{j=1}^K \beta_j < (T - K)\beta_k$ : in this case,  $A < 0$  and  $C > 0$ . Therefore,  $F(P_p) = 0$  has two distinct real roots  $P_{p_1}, P_{p_2} = \frac{-B \pm \sqrt{B^2 - 4AC}}{2A}$ . Since  $A, B < 0$ ,  $P_{p_1} = \frac{-B + \sqrt{B^2 - 4AC}}{2A} < 0$ . Also,

$$\begin{aligned}
B^2 - 4AC &= 4K^2(T - K) \frac{M}{P} \left( (T - K) \left( \frac{P}{M} + \beta_k P_t \right) + \left( \sum_{j=1}^K \beta_j \right) \left( \frac{M}{P} \beta_k P_t^2 + P_t \right) \right) \\
&< 4K^2(T - K)^2 \left( 1 + 2 \frac{M}{P} \beta_k P_t + \left( \frac{M}{P} \right)^2 \beta_k^2 P_t^2 \right).
\end{aligned} \tag{4-13}$$

This implies that

$$P_{p_2} < \frac{2K \left( \frac{M}{P} \right) P_t (\sum_{j=1}^K \beta_j - (T - K)\beta_k)}{2K^2 \left( \frac{M}{P} \right) (\sum_{j=1}^K \beta_j - (T - K)\beta_k)} = \frac{P_t}{K}. \tag{4-14}$$

Moreover, since  $B^2 - 4AC > 4K^2(\sum_{j=1}^K \beta_j)^2 \left( \left( \frac{M}{P} \right) P_t + \frac{1}{\beta_k} \right)^2$ , we have

$$P_{p_2} > \frac{2K \left( (T - K)\beta_k - \sum_{j=1}^K \beta_j \right) \frac{1}{\beta_k}}{2K^2 \left( \frac{M}{P} \right) (\sum_{j=1}^K \beta_j - (T - K)\beta_k)} = \frac{-\frac{1}{\beta_k}}{K \frac{M}{P}} \rightarrow 0 \text{ as } M \rightarrow \infty. \tag{4-15}$$

Therefore, the second root satisfies  $0 < P_{p_2} < \frac{P_t}{K}$ . Table 4-1 shows the sign table of  $F(p_p)$  for this case. As this table demonstrates, for  $0 < P_p < \frac{P_t}{K}$ , the first derivative of  $\text{SINR}_k^{\text{MRC}}$  is positive for

$P_p < P_{p_2}$ , and is negative for  $P_p > P_{p_2}$ . Therefore,  $\text{SINR}_k^{\text{MRC}}$  is a concave function with one global maximum.

2-  $\sum_{j=1}^K \beta_j > (T - K)\beta_k$ : for this case we also have  $B^2 - 4AC > 0$  and as the result,  $F(P_p)$  has two distinct real roots. Following the steps mentioned in the previous case, we can show that the first root satisfies  $0 < P_{p_1} = \frac{-B - \sqrt{B^2 - 4AC}}{2A} < \frac{P_t}{K}$ . For  $P_{p_2} = \frac{-B + \sqrt{B^2 - 4AC}}{2A}$ , we have

$$\begin{aligned} B^2 - 4AC &= 4K^2(T - K) \frac{M}{P} \left( (T - K) \left( \frac{P}{M} + \beta_k P_t \right) + \left( \sum_{j=1}^K \beta_j \right) \left( \frac{M}{P} \beta_k P_t^2 + P_t \right) \right) \\ &> 4K^2(T - K)^2 \left( 1 + 2 \frac{M}{P} \beta_k P_t + \left( \frac{M}{P} \right)^2 \beta_k^2 P_t^2 \right). \end{aligned} \quad (4-16)$$

Therefore,

$$\begin{aligned} P_{p_2} &> \frac{4K(T - K) + 2K \frac{M}{P} P_t (\sum_{j=1}^K \beta_j + (T - K)\beta_k)}{2K^2 \left( \frac{M}{P} \right) (\sum_{j=1}^K \beta_j - (T - K)\beta_k)} \\ &> \frac{2K \frac{M}{P} P_t (\sum_{j=1}^K \beta_j + (T - K)\beta_k)}{2K^2 \left( \frac{M}{P} \right) (\sum_{j=1}^K \beta_j + (T - K)\beta_k)} = \frac{P_t}{K}, \end{aligned} \quad (4-17)$$

that does not satisfy the constraints. Therefore,  $P_{p_1}$  is the only acceptable root. According to Table 4-2,  $\frac{d}{dP_p} (\text{SINR}_k^{\text{MRC}})$  is positive for  $P_p < P_{p_1}$  and is negative for  $P_p > P_{p_1}$ . Hence,  $\text{SINR}_k^{\text{MRC}}$  is a concave function with respect to  $P_p$  that has one global maximum in  $0 < P_p < \frac{P_t}{K}$ .

3)  $\sum_{j=1}^K \beta_j = (T - K)\beta_k$ : in this case,  $\frac{d}{dP_p} (\text{SINR}_k^{\text{MRC}})$  has two identical real roots  $P_{p_1} = P_{p_2} = \frac{P_t}{2K}$ . According to Table 4-3,  $\text{SINR}_k^{\text{MRC}}$  is a concave function with respect to  $P_p$  with a global maximum at  $P_p = \frac{P_t}{2K}$ .

To sum up, the  $\text{SINR}_k^{\text{MRC}}$  is always a concave function with respect to  $P_p$  when  $0 < P_p < \frac{P_t}{K}$ .

Accordingly,  $\log_2(1 + \text{SINR}_k^{\text{MRC}})$  is also a concave function. Since the summation of concave functions is always a concave function, we can conclude that the objective function defined in (4-9) is also a concave function and the proof of Theorem 4 is accomplished. ■

**Table 4-1- Sign table of  $F(\mathbf{P}_P)$  where  $\sum_{j=1}^K \beta_j < (T - K)\beta_k$**

$P_{p_1} < 0$		$0 < P_{p_2} < \frac{P_t}{K}$
$F(P_P < P_{p_1})$	$F(P_{p_1} < P_P < P_{p_2})$	$F(P_P > P_{p_2})$
-	+	-

**Table 4-2- Sign table of  $F(\mathbf{P}_P)$  where  $\sum_{j=1}^K \beta_j > (T - K)\beta_k$**

$0 < P_{p_1} < \frac{P_t}{K}$		$P_{p_2} > \frac{P_t}{K}$
$F(P_P < P_{p_1})$	$F(P_{p_1} < P_P < P_{p_2})$	$F(P_P > P_{p_2})$
+	-	+

**Table 4-3- Sign table of  $F(\mathbf{P}_P)$  where  $\sum_{j=1}^K \beta_j = (T - K)\beta_k$**

$P_{p_1} = P_{p_2} = \frac{P_t}{2K}$	
$F(P_P < P_{p_1})$	$F(P_P > P_{p_1})$
+	-

## 4.2 Simulation Results for Different Receivers

In this section, simulation results are provided that verify the mathematical analysis presented above. First, considering fixed  $\beta_k$ s, we present an example of the objective function given by (4-9) for MRC, ZF, and LMMSE receivers. Then, we evaluate the approximate expressions obtained for the achievable spectral efficiency of the receivers mentioned above. Besides, considering the different number of BS antennas and the different number of channel dimensions, the performance of our proposed power allocation scheme is studied. We also analyze and compare the optimum ratio of  $\frac{P_P}{P_u}$  for different receivers. Finally, by investigating a more practical scenario in which  $\beta_k$ s change, we evaluate the achievable spectral efficiency applying our proposed power allocation method. Note that the results presented in this section are published in [59].

In all the simulations, the users are assumed to be distributed uniformly in a hexagonal single-cell and no user is closer than  $d_h = 50$  meters to the BS. To generate the large-scale fading coefficients, that model the single-slope path loss as well as the shadowing, we use  $\beta_k = \frac{z_k}{\left(\frac{d_k}{d_h}\right)^\alpha}$ ,

where  $z_k$  is the log-normal random variable with  $\delta_{shadow} = 8dB$ ,  $d_k$  is the distance between user  $k$  and the BS, and the path loss exponent is assumed to be equal to  $\alpha = 3.8$ . The total coherence interval is considered to be  $T = 200$  in symbols that corresponds to the coherence time of 1 ms and coherence bandwidth of 200kHz. Moreover, different values for the physical parameters such as  $K$ ,  $P$ ,  $M$ , and SNR—that can be represented by  $SNR = \frac{P_t}{T}$ , assuming the noise power to be one—are considered for different simulations. Table 4-4 summarizes all the parameters used for different simulation results.

**Table 4-4- System parameters for the simulations**

Figures	$K$	$M$	$P$	SNR	$\beta$ values
Figure 4-1	15	100	30	-5dB	[13.9,3.69,6.54,3.09,28.94,64.63,6.82,8.68,13.97,6.68,14.18,13.97,1.27,44.96,7.83]× 10 <sup>-2</sup>
Figure 4-2	20	100	30	-30dB-10dB	[9.1,1.0,0.6,1.8,1.0,32.1,103.5,0.8,55.77,0.3,0.5,11.78,1.6,3.4,8.7,3.5,7.6,2.6,844.8,159.7]× 10 <sup>-3</sup>
Figure 4-3	20	200	30	-30dB-10dB	[9.1,1.0,0.6,1.8,1.0,32.1,103.5,0.8,55.77,0.3,0.5,11.78,1.6,3.4,8.7,3.5,7.6,2.6,844.8,159.7]× 10 <sup>-3</sup>
Figure 4-4	20	50-500	30	-5dB	[9.1,1.0,0.6,1.8,1.0,32.1,103.5,0.8,55.77,0.3,0.5,11.78,1.6,3.4,8.7,3.5,7.6,2.6,844.8,159.7]× 10 <sup>-3</sup>
Figure 4-5	20	50-500	30	5dB	[9.1,1.0,0.6,1.8,1.0,32.1,103.5,0.8,55.77,0.3,0.5,11.78,1.6,3.4,8.7,3.5,7.6,2.6,844.8,159.7]× 10 <sup>-3</sup>
Figure 4-6	20	50-500	30	-5dB	[9.1,1.0,0.6,1.8,1.0,32.1,103.5,0.8,55.77,0.3,0.5,11.78,1.6,3.4,8.7,3.5,7.6,2.6,844.8,159.7]× 10 <sup>-3</sup>
Figure 4-7	20	50-500	30	5dB	[9.1,1.0,0.6,1.8,1.0,32.1,103.5,0.8,55.77,0.3,0.5,11.78,1.6,3.4,8.7,3.5,7.6,2.6,844.8,159.7]× 10 <sup>-3</sup>
Figure 4-8	20	200	30-100	0dB	[9.1,1.0,0.6,1.8,1.0,32.1,103.5,0.8,55.77,0.3,0.5,11.78,1.6,3.4,8.7,3.5,7.6,2.6,844.8,159.7]× 10 <sup>-3</sup>
Figure 4-9	20	200	30-100	10dB	[9.1,1.0,0.6,1.8,1.0,32.1,103.5,0.8,55.77,0.3,0.5,11.78,1.6,3.4,8.7,3.5,7.6,2.6,844.8,159.7]× 10 <sup>-3</sup>

Figure 4-10	20	150	30, 70	-30dB-10dB	[9.1,1.0,0.6,1.8,1.0,32.1,103.5,0.8,55.77,0.3,0.5,11.78,1.6,3.4,8.7,3.5,7.6,2.6,844.8,159.7] $\times 10^{-3}$
Figure 4-11	20	150	40	0dB	500 different $\beta$ vectors corresponding to 500 Monte-Carlo simulations
Figure 4-12	20	150	40	10dB	500 different $\beta$ vectors corresponding to 500 Monte-Carlo simulations

Figure 4-1 displays an example of the objective function in (4-9) for different receivers, assuming  $P = 30$ ,  $K = 15$ , and  $M = 100$ . Note that only for this figure the radius of the hexagonal cell is assumed to be 500 meters, while for the rest of the simulation results the radius of 1000 meters is considered. As this figure demonstrates, (4-9) is a concave function. Hence, it has a global optimum solution in the interval of  $0 \leq P_p \leq \frac{P_t}{K}$  for MRC, ZF, and LMMSE receivers that can be found using a convex optimization method [68]. This optimal value of  $P_p$  is large enough to provide accurate channel estimations yet small enough to leave an adequate power for the data transmission phase.

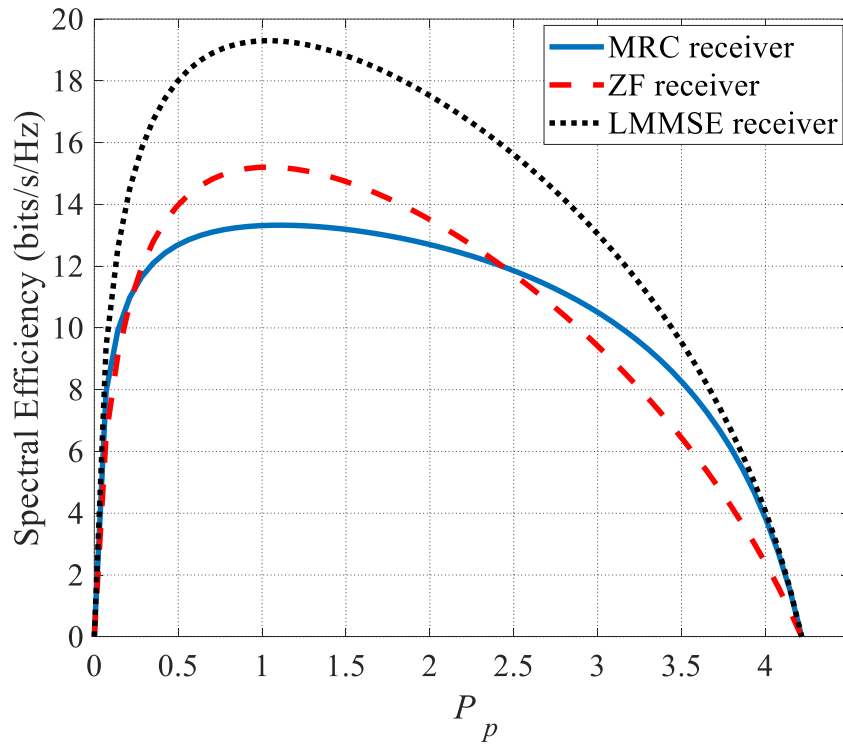


Figure 4-1- Spectral efficiency versus  $P_p$  for MRC, ZF, and LMMSE receivers (in this figure,  $\text{SNR} = -5\text{dB}$ ,  $M = 100$ , and  $P = 30$ )

To verify the accuracy of the approximate closed-form rates, Figure 4-2 and Figure 4-3 are presented. These figures compare the numerically evaluated exact spectral efficiency with the approximate spectral efficiency given by (4-1), assuming equal power  $\frac{P_t}{T}$  is allocated to data and pilot symbols. In order to obtain the semi-analytic spectral efficiency, a uniform linear array with  $\frac{d}{\lambda} = 0.3$  is considered at the BS. Moreover, the arrival angles are assumed to be uniformly distributed over  $[-\pi/2, \pi/2]$ , i.e.,  $\phi_p = -\frac{\pi}{2} + \frac{(p-1)\pi}{P}, p = 1, \dots, P$ . Both figures show that the derived approximations are very accurate. Besides, the results for different numbers of BS antennas depict that by increasing  $M$ , our approximations become even more precise and approach tight lower bounds for all the receivers. Also, for smaller numbers of BS antennas, the analytical results are more precise at lower SNR values, while they are tight for all the SNR values when  $M$  is large. To summarize, Figure 4-2 and Figure 4-3 emphasize that although the approximate expression obtained for the LMMSE receiver is more accurate, the analytical results are also very tight for MRC and ZF receivers, especially when  $M$  is large. Hence, in the following, by choosing sufficiently large  $M$  values, we will use the derived approximations for all numerical works.

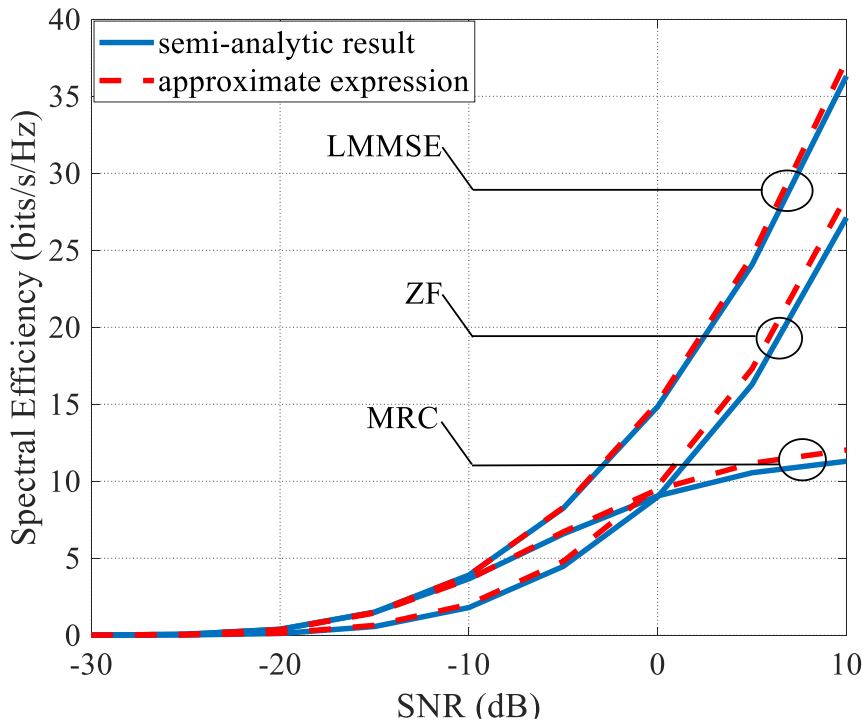


Figure 4-2- Semi-analytic spectral efficiency as well as approximate spectral efficiency (in this figure,  $M = 100$ ,  $P = 30$ , and  $P_u = P_p = \frac{P_t}{T}$ )

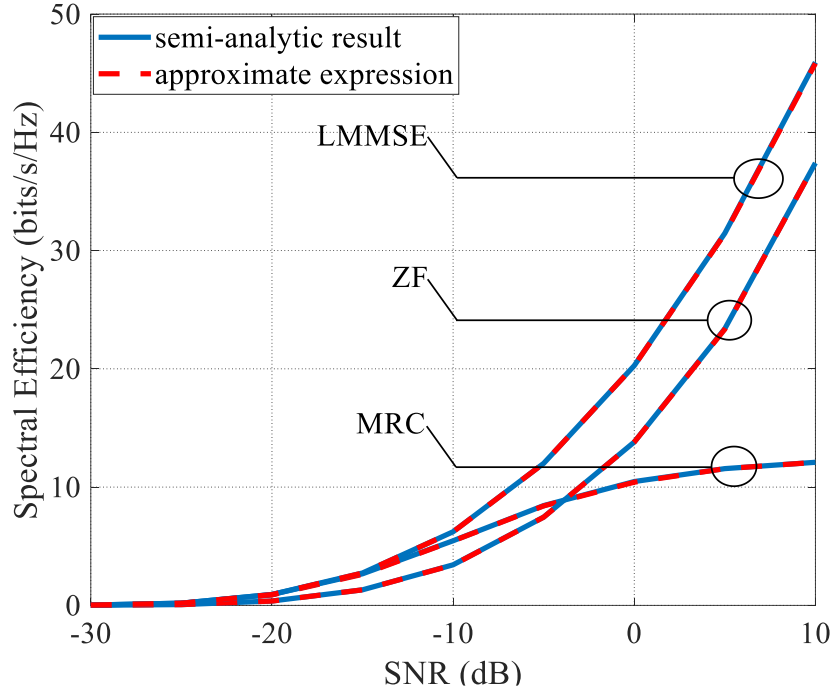


Figure 4-3- Semi-analytic spectral efficiency as well as approximate spectral efficiency (in this figure,  $M = 200$ ,  $P = 30$ , and  $P_u = P_p = \frac{P_t}{T}$ )

Figure 4-4 and Figure 4-5 show the achievable spectral efficiency versus  $M$  for different UL training durations and different SNR values. As these figures confirm, the minimum value of  $\tau$  that keeps the orthogonality among pilots is the optimal value of UL training duration in order to maximize the spectral efficiency of MRC, ZF, and LMMSE receivers. In other words, for a specific number of users in the network, the optimal number of transmitted pilots that also avoids pilot contamination is equal to the number of users.

To compare the achievable spectral efficiency of the proposed power allocation scheme to the equal power allocation, Figure 4-6 to Figure 4-9 are presented. Figure 4-6 and Figure 4-7 display spectral efficiency as a function of the number of antennas at the BS for MRC, ZF, and LMMSE receivers. Figure 4-8 and Figure 4-9 present the spectral efficiency as a function of the number of directions  $P$ . For different SNR values, they compare the proposed power allocation method with the case where  $P_u = P_p = \frac{P_t}{T}$  as in [22] for single-cell scenario (note that in [22], only MRC and ZF receivers are investigated). As these figures show, the proposed resource allocation method improves the spectral efficiency in comparison to the case where  $P_u = P_p = \frac{P_t}{T}$ . This improvement becomes more prominent as the number of BS antennas and the number of channel directions

grow. Besides, these figures display that our power allocation scheme is more efficient on LMMSE and ZF receivers than the MRC receiver, especially at higher SNR values. In addition, the results for different SNR values confirm the superiority of the LMMSE receiver in terms of the achievable spectral efficiency. They also depict that comparing to MRC and ZF, the spectral efficiency of the LMMSE receiver has the least sensitivity to the  $P$  increment. In other words, the enhancement of spectral efficiency achieved by increasing the number of directions has a very slight slope for the LMMSE receiver.

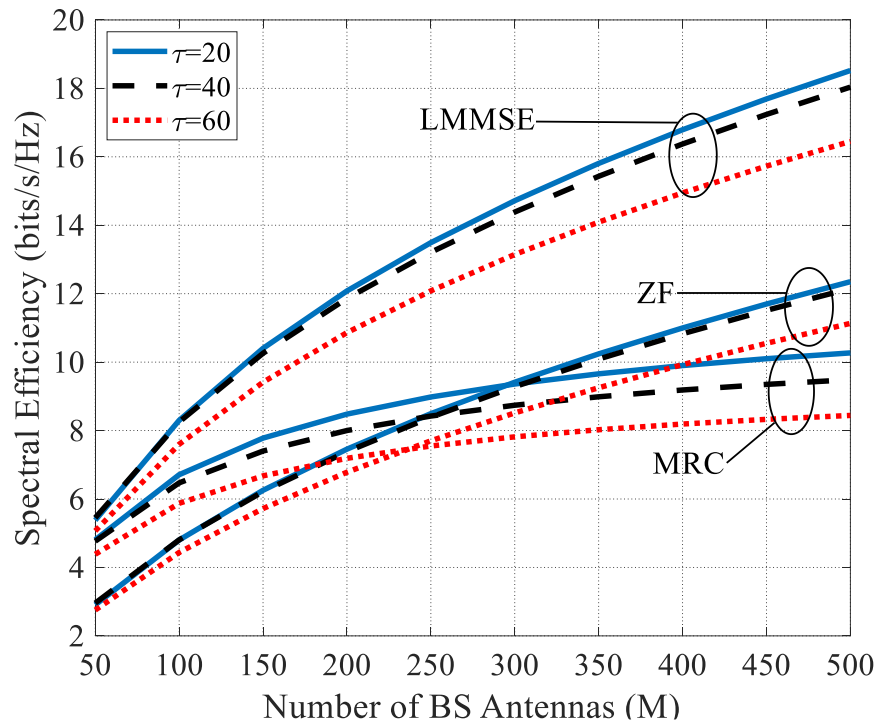


Figure 4-4- Spectral efficiency versus the number of BS antennas for different UL training durations (in this figure, SNR =  $-5dB$  and  $P = 30$ )

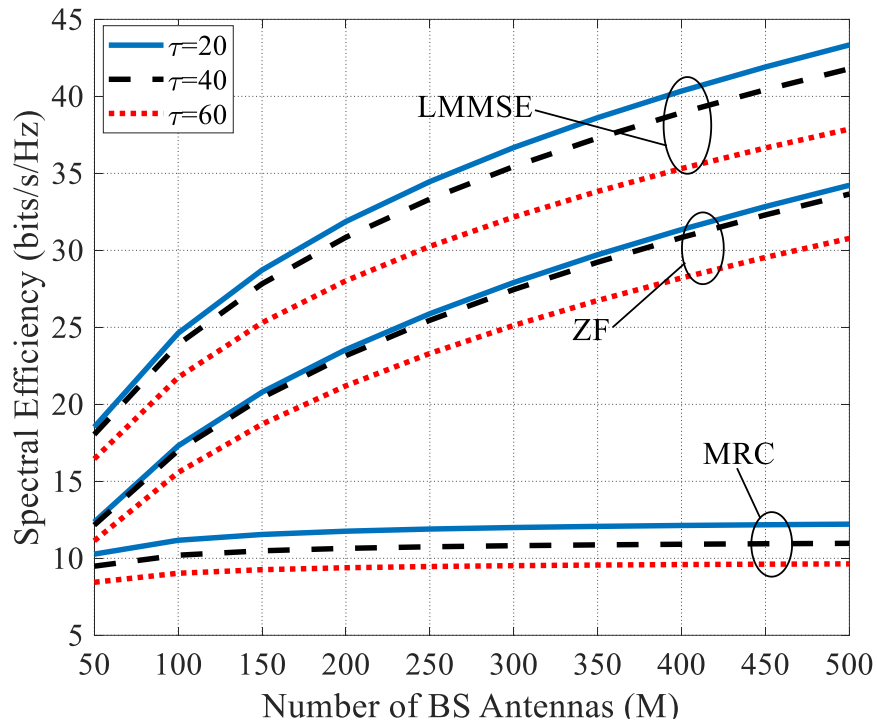


Figure 4-5- Spectral efficiency versus the number of BS antennas for different UL training durations (in this figure, SNR = 5dB and  $P = 30$ )

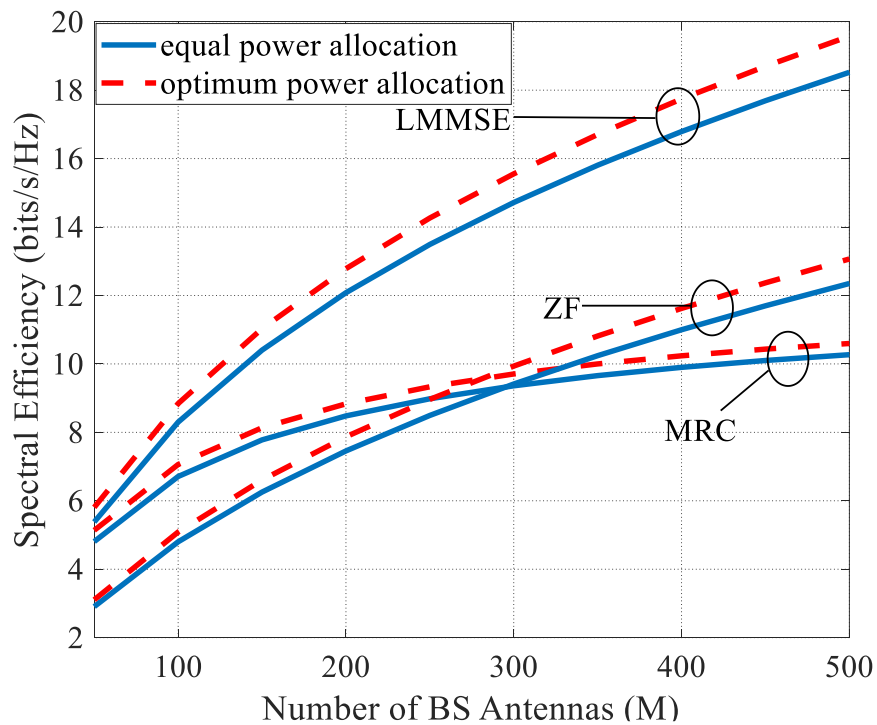


Figure 4-6- Spectral efficiency versus the number of BS antennas with equal power and optimum power allocation (in this figure, SNR = -5dB and  $P = 30$ )

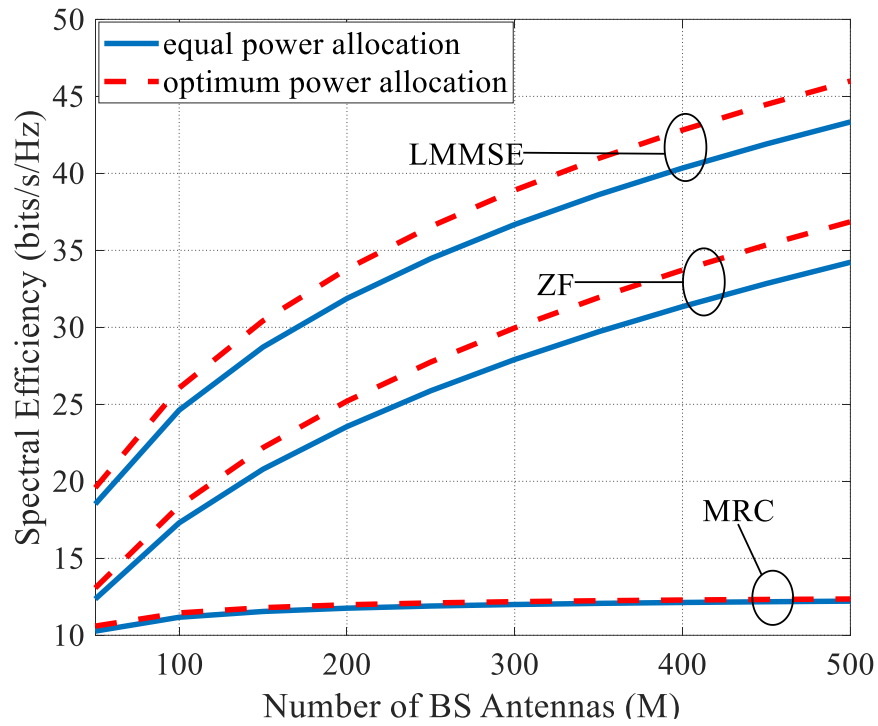


Figure 4-7- Spectral efficiency versus the number of BS antennas with equal power and optimum power allocation (in this figure, SNR = 5dB and  $P = 30$ )

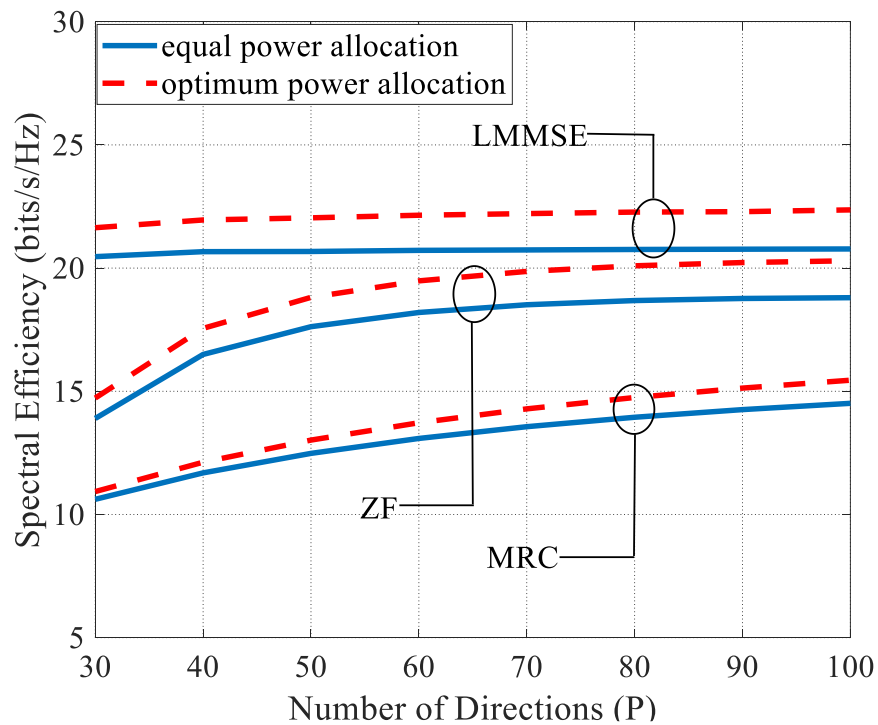


Figure 4-8- Spectral efficiency versus the number of directions with equal power and optimum power allocation (in this figure, SNR = 0dB and  $M = 200$ )

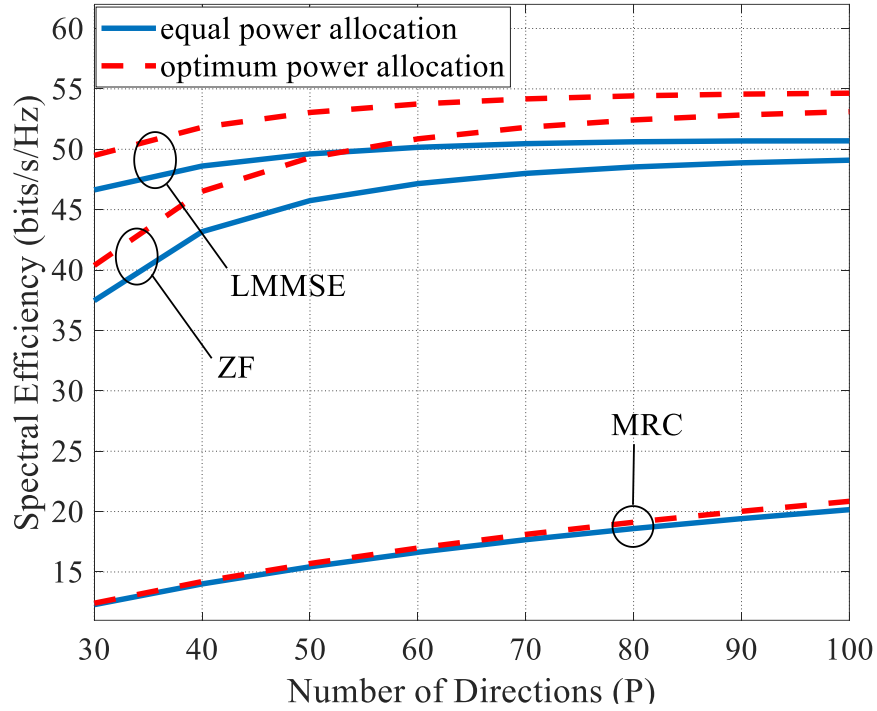


Figure 4-9- Spectral efficiency versus the number of directions with equal power and optimum power allocation (in this figure, SNR = 10dB and M = 200)

Figure 4-10 displays the optimal ratio of the pilot symbol power to the data symbol power for different values of SNR. It can be concluded that at low values of SNR, more power should be spent for the training phase, while at higher SNR values, the required power for the training phase decreases, and allocating more power to the data transmission phase optimizes the spectral efficiency. For instance, at SNR=-30dB and  $P = 70$ , the optimum ratio equals  $\frac{P_p}{P_u} = 7.785$  that results in  $\tau P_p = 20 \times 7.785 \times P_u \approx (200 - 20)P_u$ . This means that in order to achieve the optimal spectral efficiency at low SNR values, the total training power and data transmission power should be almost equal. While by SNR increment, allocating more power to the data transmission phase optimizes the spectral efficiency. This complies with the fact that increasing the SNR value (or equivalently decreasing the noise power) results in more accurate channel estimations. Figure 4-10 also demonstrates that for all the discussed receivers, increasing the dimensionality of the channel leads to a larger optimum training power.

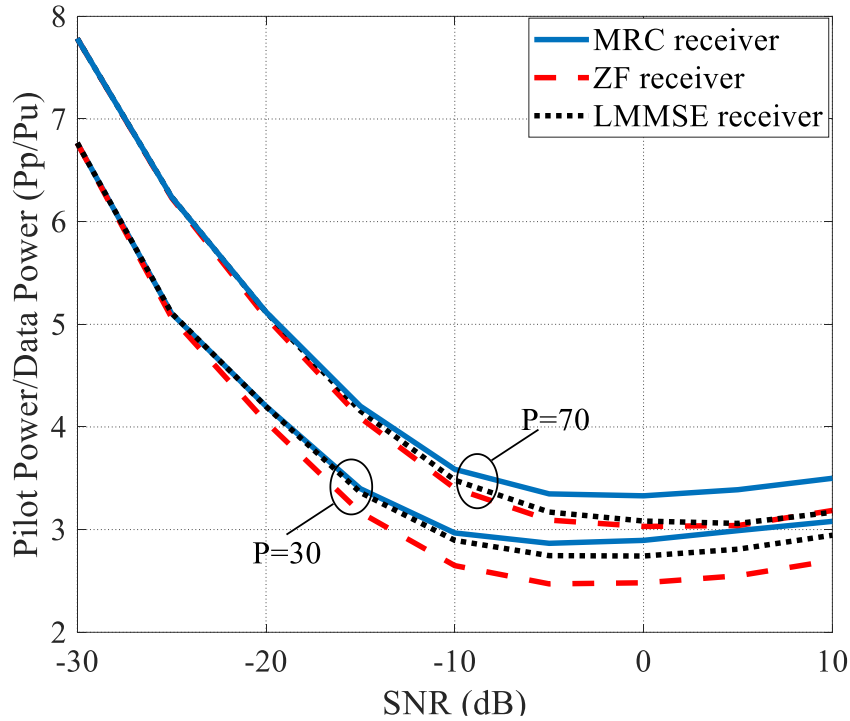


Figure 4-10- Optimal pilot power to data power ratio versus the SNR value (in this figure,  $M = 150$ )

Finally, Figure 4-11 and Figure 4-12 compare the cumulative distribution function (CDF) of the spectral efficiency at different SNR values, considering the optimal power allocation scheme as well as the equal power allocation. To generate these figures, 500 Monte-Carlo simulations are run where the position of users in the cell changes randomly in each simulation snapshot. As expected, regardless of the SNR value, applying the proposed power allocation scheme always improves the spectral efficiency of the network. However, Figure 4-12 emphasizes that at high SNR values, the proposed power allocation scheme offers more efficiency for ZF and LMMSE receivers. It is worth noting that our proposed power allocation scheme is based on large-scale fading coefficients. Hence, the BS can find the optimum value of  $\frac{P_p}{P_u}$  once and apply it during several coherence intervals, where the large-scale fading coefficients remain unchanged. This decreases the computational time as well as the required overhead significantly.

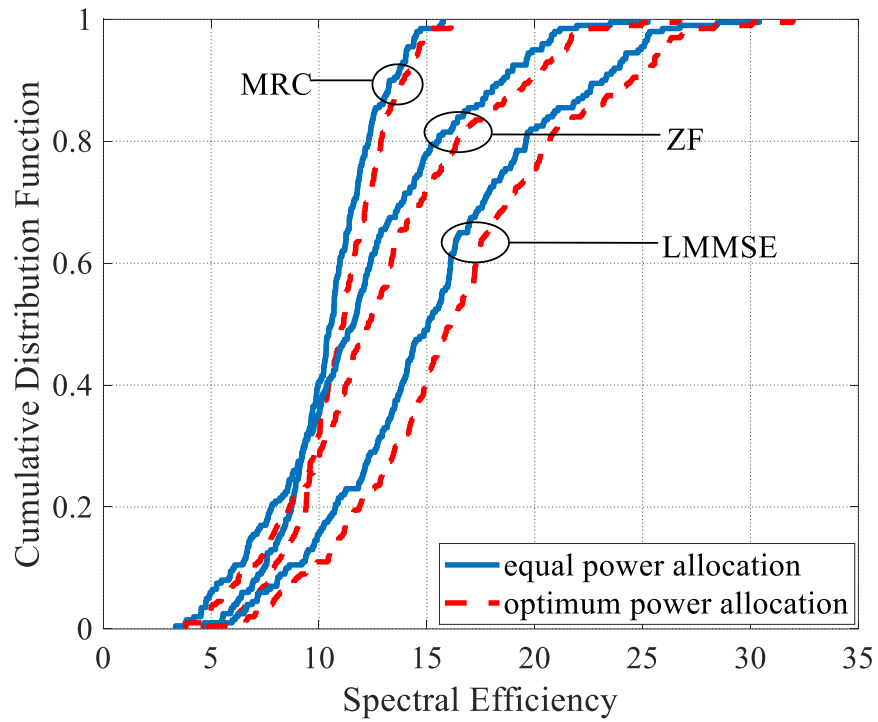


Figure 4-11- CDF of spectral efficiency with and without optimal power allocation (in this figure, SNR = 0dB,  $P = 40$  and  $M = 150$ )

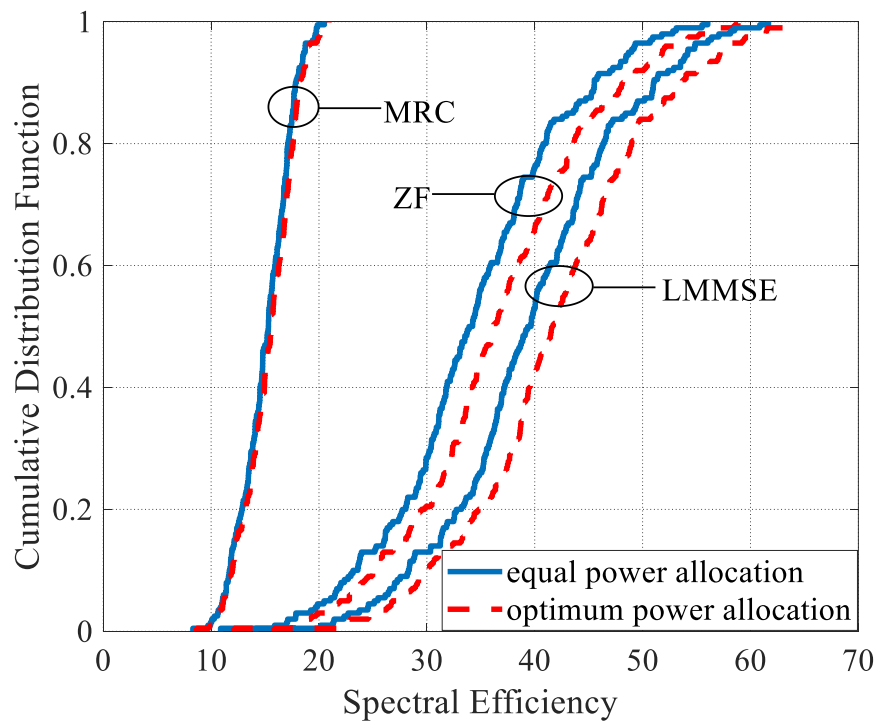


Figure 4-12- CDF of spectral efficiency with and without optimal power allocation (in this figure, SNR = 10dB,  $P = 40$  and  $M = 150$ )

### 4.3 Concluding Remarks

In summary, in this chapter, we developed a closed-form approximation for the spectral efficiency of finite-dimensional multiuser massive MIMO, assuming MRC, ZF, and LMMSE receivers at the BS. We also analytically proved the concavity of the developed spectral efficiency with respect to the pilot symbol power in a theorem. Besides, we investigated the effect of several physical parameters on achievable spectral efficiency. These parameters include the number of users, the number of antennas at the BS, the number of channel directions, different SNR values, different users' locations ( $\beta$ ), UL training duration, pilot power, and data power. Our simulation results confirmed the accuracy of the derived approximate spectral efficiencies. We also showed the spectral efficiency enhancement achieved through allocating optimal power to pilot and data transmission and presented the impact of SNR value on the optimal ratio of pilot power to data power.

## Chapter 5: CONCLUSIONS AND THE FUTURE DIRECTION

### 5.1 Conclusions

In this thesis, we propose a method for optimally dividing the resources between data and pilot sequences to improve the spectral efficiency in the UL transmission of multiuser massive MIMO. More specifically, we consider a channel model with a finite number of dimensions in a single-cell massive MIMO system. We assume the angular domain has limited independent directions and by presenting the array steering vector for each one of these directions, we describe the channel matrix between the BS and  $K$  users as the multiplication of the array steering matrix and the propagation coefficients matrix. We further assume that the channel coefficients are estimated by the BS through the UL pilot transmission prior to the data transmission phase. By considering the effect of channel estimation error into account, we derive the achievable UL rate of users, assuming linear receivers such as MRC, ZF, and LMMSE are employed at the BS.

Moreover, assuming the BS is equipped with a uniform linear antenna array, we derive closed-form approximations for the achievable UL rate of MRC, ZF, and LMMSE receivers and analytically prove the accuracy of these approximate expressions. We show that for a large number of antennas at the BS, these derived approximate closed-forms are very tight and approach lower bounds for all the receivers. Then, we develop an approximation for spectral efficiency based on these rates that reduces the computational complexity. We further prove the concavity of this approximate spectral efficiency with respect to pilot symbol power and propose a resource allocation scheme in which the pilot power, data power, and training duration are jointly selected in order to maximize spectral efficiency.

To evaluate the performance of the proposed resource allocation scheme, we present several simulation results. The results affirm that the proposed resource allocation scheme can significantly improve spectral efficiency and outperforms the case with equal data and pilot symbols power. We also show that the performance of the proposed method with LMMSE and ZF receivers is much more significant than that with the MRC receiver. Finally, we conclude that increasing the number of dimensions as well as the number of BS antennas enhances the spectral efficiency improvement resulted from our proposed resource allocation.

## 5.2 Future Works

Our research work in this thesis has mainly focused on spectral efficiency maximization in a single-cell multiuser massive MIMO system. However, there are additional studies that can be accomplished along the lines developed in this thesis. Some of these possible future studies are briefly presented in the following.

### 5.2.1 *Multiuser Massive MIMO with Various Allocated Resources*

In this thesis, we assumed that all the users in the network have the same amount of resources (the same power budget as well as the same number of UL pilot symbols) and distribute them in between UL pilot and data transmission phases in the same manner. In a more general scenario, we can extend the proposed method in this thesis to the case in which users have different amounts of resources. For such scenarios, maximizing the spectral efficiency through joint optimal pilot and data resource allocation results in an NP-hard optimization problem. Hence, novel iterative algorithms are required to find the local maximum points [58]. Another possible solution for the real-time implementation of this joint resource allocation scheme is to develop a neural network that is able to predict the optimal pilot and data powers [69].

### 5.2.2 *Multi-cell Multiuser Massive MIMO Systems*

In multi-cell scenarios, the transmission activities (include pilot transmission, UL data transmission, and DL data transmission) of different cells happen synchronously and since there is no cell-to-cell cooperation, inter-cell interference occurs. Hence, the system model should be refined to take the pilot contamination as well as the inter-cell interference effect into consideration. New bounds on the achievable spectral efficiencies should be derived and then, the proposed resource allocation method can be investigated to maximize the spectral efficiency in the network.

### 5.2.3 *Resource Allocation in Cell-free Massive MIMO*

Cell-free massive MIMO is a topology for implementing massive MIMO networks. Unlike collocated massive MIMO, in cell-free massive MIMO, the antennas (APs) are distributed randomly to maximize fairness in the network. The investigations in [70] regarding the impact of DL pilot training in cell-free massive MIMO have indicated that per-user net throughput, especially in low-density networks, can be remarkably improved by employing DL training. This

result emphasizes that due to the less pronounced channel hardening effect, DL pilots are more necessary to be used in cell-free massive MIMO than collocated massive MIMO. Therefore, considering pilot transmission in both UL and DL, the achievable DL rate of users can be first found, and then, by applying the optimal resource allocation scheme presented in this thesis, the DL achievable spectral efficiency of cell-free massive MIMO can be improved.

## Chapter 6: APPENDICES

### 6.1 Appendix I

Using the approximation given by (3-19),  $\hat{\mathbf{l}}_k^H [(\sum_{j=1}^K \beta_j) \mathbf{U}\mathbf{U}^H - \mathbf{cov}(\hat{\mathbf{l}}_k)] \hat{\mathbf{l}}_k$  in the denominator of (3-16) can be approximated by

$$\begin{aligned}
 & \hat{\mathbf{l}}_k^H \left[ \left( \sum_{j=1}^K \beta_j \right) \mathbf{U}\mathbf{U}^H - \mathbf{cov}(\hat{\mathbf{l}}_k) \right] \hat{\mathbf{l}}_k \\
 &= \hat{\mathbf{l}}_k^H \left[ \left( \sum_{j=1}^K \beta_j \right) \mathbf{U}\mathbf{U}^H - \tau_{P_P} \beta_k^2 \mathbf{U} (\tau_{P_P} \mathbf{U}^H \mathbf{U} \beta_k + \mathbf{I}_P)^{-1} \mathbf{U}^H \mathbf{U}\mathbf{U}^H \right] \hat{\mathbf{l}}_k \\
 &\approx \hat{\mathbf{l}}_k^H \left[ \left( \sum_{j=1}^K \beta_j \right) - \frac{\tau_{P_P} \beta_k^2 \left( \frac{M}{P} \right)}{\tau_{P_P} \beta_k \left( \frac{M}{P} \right) + 1} \right] \mathbf{U}\mathbf{U}^H \hat{\mathbf{l}}_k \tag{6-1} \\
 &= \left[ \left( \sum_{j=1}^K \beta_j \right) - \frac{\tau_{P_P} \beta_k^2 \left( \frac{M}{P} \right)}{\tau_{P_P} \beta_k \left( \frac{M}{P} \right) + 1} \right] \beta_k \hat{\mathbf{h}}_k^H \mathbf{U}^H \mathbf{U}\mathbf{U}^H \mathbf{U} \hat{\mathbf{h}}_k \\
 &\approx \left[ \left( \sum_{j=1}^K \beta_j \right) - \frac{\tau_{P_P} \beta_k^2 \left( \frac{M}{P} \right)}{\tau_{P_P} \beta_k \left( \frac{M}{P} \right) + 1} \right] \beta_k \left( \frac{M}{P} \right)^2 \|\hat{\mathbf{h}}_k\|^2.
 \end{aligned}$$

Moreover, we have

$$\|\hat{\mathbf{l}}_k\|^4 = (\beta_k \hat{\mathbf{h}}_k^H \mathbf{U}^H \mathbf{U} \hat{\mathbf{h}}_k)^2 \approx \beta_k^2 \left( \frac{M}{P} \right)^2 \|\hat{\mathbf{h}}_k\|^4. \tag{6-2}$$

Substituting (6-1) and (6-2) into (3-16) results in

$$R_k^{MRC} \approx \mathbb{E} \left\{ \log_2 \left( 1 + \frac{1}{\left[ \left( \sum_{j=1}^K \beta_j \right) - \frac{\tau_{P_P} \beta_k^2 \left( \frac{M}{P} \right)}{\tau_{P_P} \beta_k \left( \frac{M}{P} \right) + 1} \right] \frac{1}{P_u M} \beta_k \|\hat{\mathbf{h}}_k\|^2} \right) \right\}, \tag{6-3}$$

that becomes exact as  $M \rightarrow \infty$ . Besides, according to Jensen's inequality and because  $\log_2(1 + \frac{1}{x})$  is a convex function, we conclude that  $\mathbb{E} \left\{ \log_2(1 + \frac{1}{x}) \right\} \geq \log_2(1 + \frac{1}{\mathbb{E}\{x\}})$ . Therefore, a lower bound for the UL rate given by (6-3) can be obtained as

$$R_k^{MRC} \geq \log_2 \left( 1 + \frac{1}{\left[ (\sum_{j=1}^K \beta_j) - \frac{\tau P_P \beta_k^2 \left(\frac{M}{P}\right)}{\tau P_P \beta_k \left(\frac{M}{P}\right) + 1} + \frac{1}{P_u} \frac{P}{M} \right] \frac{1}{\beta_k} \mathbb{E} \left\{ \frac{1}{\|\hat{\mathbf{h}}_k\|^2} \right\}} \right). \quad (6-4)$$

Applying the properties of central complex Wishart matrix [71] and considering  $\mathbf{cov}(\hat{\mathbf{h}}_k) \approx \frac{\tau P_P \beta_k \left(\frac{M}{P}\right)}{\tau P_P \beta_k \left(\frac{M}{P}\right) + 1} \mathbf{I}_P$ , we have

$$\mathbb{E} \left\{ \frac{1}{\|\hat{\mathbf{h}}_k\|^2} \right\} = \mathbb{E} \left\{ \mathbf{tr} \left( (\|\hat{\mathbf{h}}_k\|^2)^{-1} \right) \right\} = \frac{\tau P_P \beta_k \left(\frac{M}{P}\right) + 1}{\tau P_P \beta_k \left(\frac{M}{P}\right)} \times \frac{1}{P-1}, \quad (6-5)$$

for  $P \geq 2$ . Substituting (6-5) into (6-4) results in the approximate rate given by Theorem 1.

To analytically prove the accuracy of the derived closed-form rate, let's also find an upper bound for (3-16). According to Jensen's inequality for concave functions, we have  $\mathbb{E} \left\{ \log_2 \left( 1 + \frac{1}{x} \right) \right\} \geq \log_2 \left( 1 + \mathbb{E} \left\{ \frac{1}{x} \right\} \right)$ . This results in

$$R_k^{MRC} \leq \log_2 \left( 1 + \mathbb{E} \left\{ \frac{1}{\left[ (\sum_{j=1}^K \beta_j) - \frac{\tau P_P \beta_k^2 \left(\frac{M}{P}\right)}{\tau P_P \beta_k \left(\frac{M}{P}\right) + 1} + \frac{1}{P_u} \frac{P}{M} \right] \frac{1}{\beta_k} \frac{1}{\|\hat{\mathbf{h}}_k\|^2}} \right\} \right) \quad (6-6)$$

$$= \log_2 \left( 1 + \frac{\mathbb{E} \left\{ \|\hat{\mathbf{h}}_k\|^2 \right\}}{\left[ (\sum_{j=1}^K \beta_j) - \frac{\tau P_P \beta_k^2 \left(\frac{M}{P}\right)}{\tau P_P \beta_k \left(\frac{M}{P}\right) + 1} + \frac{1}{P_u} \frac{P}{M} \right] \frac{1}{\beta_k}} \right),$$

where the expectation term can be given by

$$\mathbb{E} \left\{ \|\hat{\mathbf{h}}_k\|^2 \right\} = \mathbf{tr} \left( \mathbf{cov}(\hat{\mathbf{h}}_k) \right) \approx \mathbf{tr} \left( \frac{\tau P_P \beta_k \left(\frac{M}{P}\right)}{\tau P_P \beta_k \left(\frac{M}{P}\right) + 1} \mathbf{I}_P \right) = \frac{\tau P_P \beta_k \left(\frac{M}{P}\right)}{\tau P_P \beta_k \left(\frac{M}{P}\right) + 1} P. \quad (6-7)$$

Hence, we conclude that

$$\log_2(1 + \alpha(P - 1)) \leq R_k^{MRC} \leq \log_2(1 + \alpha P), \quad (6-8)$$

where  $\alpha = \frac{\tau P_p \frac{M}{P} \beta_k^2}{\left[ \left( \sum_{j=1}^K \beta_j \right) - \frac{\tau P_p \beta_k^2 \left( \frac{M}{P} \right)}{\tau P_p \beta_k \left( \frac{M}{P} \right) + 1} + \frac{1}{P_u M} \right] \left( \tau P_p \frac{M}{P} \beta_k + 1 \right)}$ . When  $M$  is large,  $\left[ \left( \sum_{j=1}^K \beta_j \right) - \frac{\tau P_p \beta_k^2 \left( \frac{M}{P} \right)}{\tau P_p \beta_k \left( \frac{M}{P} \right) + 1} + \frac{1}{P_u M} \right] \rightarrow \left( \sum_{j=1, j \neq k}^K \beta_j \right)$  and therefore,  $\alpha \rightarrow \frac{\beta_k}{\left( \sum_{j=1, j \neq k}^K \beta_j \right)}$  that has a small value. This means that the

upper bound in (6-8) becomes very close to the lower bound that proves the accuracy of the obtained closed-form ergodic rate. Hence, the proof of Theorem 1 is completed. ■

## 6.2 Appendix II

By using  $\frac{1}{M} \mathbf{U}^H \mathbf{U} \approx \frac{1}{P} \mathbf{I}_P$  for large values of  $M$ ,  $\mathbf{cov}(\boldsymbol{\varepsilon}_j)$  in (3-22) can be approximated by

$$\mathbf{cov}(\boldsymbol{\varepsilon}_j) \approx \left( \beta_j - \frac{\tau P_p \beta_j^2 \left( \frac{M}{P} \right)}{\tau P_p \beta_j \left( \frac{M}{P} \right) + 1} \right) \mathbf{U} \mathbf{U}^H, \quad (6-9)$$

And accordingly,

$$\begin{aligned} \hat{\mathbf{L}}^H \mathbf{cov}(\boldsymbol{\varepsilon}_j) \hat{\mathbf{L}} &\approx \left( \beta_j - \frac{\tau P_p \beta_j^2 \left( \frac{M}{P} \right)}{\tau P_p \beta_j \left( \frac{M}{P} \right) + 1} \right) \mathbf{D}^{\frac{1}{2}} \hat{\mathbf{H}}^H \mathbf{U}^H \mathbf{U} \mathbf{U}^H \hat{\mathbf{H}} \mathbf{D}^{\frac{1}{2}} \\ &\approx \left( \frac{M}{P} \right)^2 \left( \frac{\beta_j}{\tau P_p \beta_j \left( \frac{M}{P} \right) + 1} \right) \mathbf{D}^{\frac{1}{2}} \hat{\mathbf{H}}^H \hat{\mathbf{H}} \mathbf{D}^{\frac{1}{2}}. \end{aligned} \quad (6-10)$$

Also, we have

$$\left( \hat{\mathbf{L}}^H \hat{\mathbf{L}} \right)^{-1} = \left( \mathbf{D}^{\frac{1}{2}} \hat{\mathbf{H}}^H \mathbf{U}^H \mathbf{U} \hat{\mathbf{H}} \mathbf{D}^{\frac{1}{2}} \right)^{-1} \approx \left( \frac{P}{M} \right) \left( \mathbf{D}^{\frac{1}{2}} \hat{\mathbf{H}}^H \hat{\mathbf{H}} \mathbf{D}^{\frac{1}{2}} \right)^{-1}. \quad (6-11)$$

As the result,  $\left( \hat{\mathbf{L}}^H \hat{\mathbf{L}} \right)^{-1} \hat{\mathbf{L}}^H \mathbf{cov}(\boldsymbol{\varepsilon}_j) \hat{\mathbf{L}} \left( \hat{\mathbf{L}}^H \hat{\mathbf{L}} \right)^{-1}$  in the denominator of (3-21) can be rewritten as

$$\left( \hat{\mathbf{L}}^H \hat{\mathbf{L}} \right)^{-1} \hat{\mathbf{L}}^H \mathbf{cov}(\boldsymbol{\varepsilon}_j) \hat{\mathbf{L}} \left( \hat{\mathbf{L}}^H \hat{\mathbf{L}} \right)^{-1} \approx \left( \frac{\beta_j}{\tau P_p \beta_j \left( \frac{M}{P} \right) + 1} \right) \left( \mathbf{D}^{\frac{1}{2}} \hat{\mathbf{H}}^H \hat{\mathbf{H}} \mathbf{D}^{\frac{1}{2}} \right)^{-1}. \quad (6-12)$$

Substituting (6-12) and (6-11) into (3-21) simplifies the denominator to

$$\begin{aligned} &\sum_{j=1}^K \left[ \left( \hat{\mathbf{L}}^H \hat{\mathbf{L}} \right)^{-1} \hat{\mathbf{L}}^H \mathbf{cov}(\boldsymbol{\varepsilon}_j) \hat{\mathbf{L}} \left( \hat{\mathbf{L}}^H \hat{\mathbf{L}} \right)^{-1} \right]_{kk} + \frac{1}{P_u} \left[ \left( \hat{\mathbf{L}}^H \hat{\mathbf{L}} \right)^{-1} \right]_{kk} \\ &\approx \left[ \left( \mathbf{D}^{\frac{1}{2}} \hat{\mathbf{H}}^H \hat{\mathbf{H}} \mathbf{D}^{\frac{1}{2}} \right)^{-1} \right]_{kk} \left( \frac{P}{M} \frac{1}{P_u} + \sum_{j=1}^K \frac{\beta_j}{\tau P_p \beta_j \left( \frac{M}{P} \right) + 1} \right). \end{aligned} \quad (6-13)$$

By using Jensen's inequality for the convex function  $\log_2(1 + \frac{1}{x})$ , a lower bound for the achievable UL rate can be obtained as

$$R_k^{ZF} \geq \log_2 \left( 1 + \frac{1}{\left( \frac{P}{M} \frac{1}{P_u} + \sum_{j=1}^K \frac{\beta_j}{\tau_{P_P} \beta_j \left( \frac{M}{P} \right) + 1} \right) \mathbb{E} \left\{ \left[ \left( \mathbf{D}^{\frac{1}{2}} \hat{\mathbf{H}}^H \hat{\mathbf{H}} \mathbf{D}^{\frac{1}{2}} \right)^{-1} \right]_{kk} \right\}} \right). \quad (6-14)$$

The expectation term  $\mathbb{E} \left\{ \left[ \left( \mathbf{D}^{\frac{1}{2}} \hat{\mathbf{H}}^H \hat{\mathbf{H}} \mathbf{D}^{\frac{1}{2}} \right)^{-1} \right]_{kk} \right\}$  in (6-14) for  $P \geq K + 1$  can be given by

$$\mathbb{E} \left\{ \left[ \left( \mathbf{D}^{\frac{1}{2}} \hat{\mathbf{H}}^H \hat{\mathbf{H}} \mathbf{D}^{\frac{1}{2}} \right)^{-1} \right]_{kk} \right\} = \frac{1}{\beta_k K} \left( \frac{\tau_{P_P} \beta_k \left( \frac{M}{P} \right) + 1}{\tau_{P_P} \beta_k \left( \frac{M}{P} \right)} \times \frac{K}{P - K} \right), \quad (6-15)$$

where the last equation is derived by using the properties of central complex Wishart matrices (the elements of  $\hat{\mathbf{H}}$  are zero mean Gaussian random variables and  $\mathbf{cov}(\hat{\mathbf{h}}_k) \approx \frac{\tau_{P_P} \beta_k \left( \frac{M}{P} \right)}{\tau_{P_P} \beta_k \left( \frac{M}{P} \right) + 1} \mathbf{I}_P$ ) [71].

Finally, substituting (6-15) into (6-14) results in the closed-form rate given by Theorem 2.

The accuracy of the obtained closed-form rate can be justified according to the Lemma 1 in [39]. This Lemma emphasizes that for any  $X$  and  $Y$  that are sums of nonnegative random variables, we can have  $\mathbb{E}\{\log_2(1 + \frac{X}{Y})\} \approx \log_2(1 + \frac{\mathbb{E}\{X\}}{\mathbb{E}\{Y\}})$ . Similarly, in this context with  $X = 1$  and

$Y = \left( \frac{P}{M} \frac{1}{P_u} + \sum_{j=1}^K \frac{\beta_j}{\tau_{P_P} \beta_j \left( \frac{M}{P} \right) + 1} \right) \left[ \left( \mathbf{D}^{\frac{1}{2}} \hat{\mathbf{H}}^H \hat{\mathbf{H}} \mathbf{D}^{\frac{1}{2}} \right)^{-1} \right]_{kk}$ , the closed-form approximate UL is very close

to the exact UL ergodic rate and the proof of Theorem 2 is completed. ■

### 6.3 Appendix III

According to Woodbury matrix identity, we have

$$\underbrace{[\hat{\mathbf{L}}\hat{\mathbf{L}}^H + \sum_{j=1}^K \mathbf{cov}(\boldsymbol{\varepsilon}_j) + \frac{1}{P_u} \mathbf{I}_M]}_{\boldsymbol{\Upsilon}}^{-1} = \boldsymbol{\Upsilon}^{-1} - \boldsymbol{\Upsilon}^{-1} \hat{\mathbf{L}} (\mathbf{I}_K + \hat{\mathbf{L}}^H \boldsymbol{\Upsilon}^{-1} \hat{\mathbf{L}})^{-1} \hat{\mathbf{L}}^H \boldsymbol{\Upsilon}^{-1}. \quad (6-16)$$

Moreover,

$$\begin{aligned}
\hat{\mathbf{L}}^H [\hat{\mathbf{L}}\hat{\mathbf{L}}^H + \sum_{j=1}^K \mathbf{cov}(\boldsymbol{\varepsilon}_j) + \frac{1}{P_u} \mathbf{I}_M]^{-1} \hat{\mathbf{L}} \\
= \hat{\mathbf{L}}^H \boldsymbol{\Upsilon}^{-1} \hat{\mathbf{L}} - \hat{\mathbf{L}}^H \boldsymbol{\Upsilon}^{-1} \hat{\mathbf{L}} (\mathbf{I}_K + \hat{\mathbf{L}}^H \boldsymbol{\Upsilon}^{-1} \hat{\mathbf{L}})^{-1} \hat{\mathbf{L}}^H \boldsymbol{\Upsilon}^{-1} \hat{\mathbf{L}} \\
= (\mathbf{I}_K + (\hat{\mathbf{L}}^H \boldsymbol{\Upsilon}^{-1} \hat{\mathbf{L}})^{-1})^{-1} = \mathbf{I}_K - (\mathbf{I}_K + \hat{\mathbf{L}}^H \boldsymbol{\Upsilon}^{-1} \hat{\mathbf{L}})^{-1}.
\end{aligned} \tag{6-17}$$

Substituting (6-17) into the denominator of (3-25) yields

$$R_k^{LMMSE} = \mathbb{E} \left\{ \log_2 \left( \frac{1}{[(\mathbf{I}_K + \hat{\mathbf{L}}^H \boldsymbol{\Upsilon}^{-1} \hat{\mathbf{L}})^{-1}]_{kk}} \right) \right\}. \tag{6-18}$$

Moreover, using the approximation given by (3-19) results in  $\sum_{j=1}^K \mathbf{cov}(\boldsymbol{\varepsilon}_j) \approx (\sum_{j=1}^K \frac{\beta_j}{\tau P_p \beta_j \frac{M}{P} + 1}) \mathbf{U}\mathbf{U}^H$  for large values of  $M$ . Therefore,

$$\begin{aligned}
\boldsymbol{\Upsilon}^{-1} &\approx \left[ \left( \sum_{j=1}^K \frac{\beta_j}{\tau P_p \beta_j \frac{M}{P} + 1} \right) \mathbf{U}\mathbf{U}^H + \frac{1}{P_u} \mathbf{I}_M \right]^{-1} \\
&= P_u \mathbf{I}_M - P_u^2 \left( \sum_{j=1}^K \frac{\beta_j}{\tau P_p \beta_j \frac{M}{P} + 1} \right) \mathbf{U} \left( \mathbf{I}_P + P_u \left( \sum_{j=1}^K \frac{\beta_j}{\tau P_p \beta_j \frac{M}{P} + 1} \right) \mathbf{U}^H \mathbf{U} \right)^{-1} \mathbf{U}^H \\
&\approx P_u \mathbf{I}_M - \frac{P_u^2 \left( \sum_{j=1}^K \frac{\beta_j}{\tau P_p \beta_j \frac{M}{P} + 1} \right)}{1 + P_u \frac{M}{P} \left( \sum_{j=1}^K \frac{\beta_j}{\tau P_p \beta_j \frac{M}{P} + 1} \right)} \mathbf{U}\mathbf{U}^H.
\end{aligned} \tag{6-19}$$

Besides, we have  $\hat{\mathbf{L}}^H \boldsymbol{\Upsilon}^{-1} \hat{\mathbf{L}} \stackrel{(3-19)}{\approx} \left( \frac{P_u \frac{M}{P}}{1 + P_u \frac{M}{P} \sum_{j=1}^K \frac{\beta_j}{\tau P_p \beta_j \frac{M}{P} + 1}} \right) \mathbf{D}^{1/2} \hat{\mathbf{H}}^H \hat{\mathbf{H}} \mathbf{D}^{1/2}$ . Accordingly, the achievable

UL ergodic rate of LMMSE receiver can be approximated by

$$R_k^{LMMSE} \approx \mathbb{E} \left\{ \log_2 \left( 1 + \frac{1}{\gamma_k} \right) \right\}, \tag{6-20}$$

where  $\gamma_k = \frac{1}{\left[ \left( \mathbf{I}_K + \left( \frac{P u^M}{1 + P u^M \sum_{j=1}^K \frac{\beta_j}{\tau P \rho \beta_j^{M+1}}} \right) \mathbf{D}^{1/2} \hat{\mathbf{H}}^H \hat{\mathbf{H}} \mathbf{D}^{1/2} \right)^{-1} \right]_{kk}} - 1$ . This approximation of the rate is exact

when  $M \rightarrow \infty$ . Besides, by using Jensen's inequality, we have

$$R_k^{LMMSE} \geq \log_2 \left( 1 + \frac{1}{\mathbb{E} \left\{ \frac{1}{\gamma_k} \right\}} \right). \quad (6-21)$$

The PDF of  $\gamma_k$  can be approximated by the Gamma distribution  $G(\alpha_k, \theta_k)$  such that  $p_{\gamma_k}(x) = \frac{x^{\alpha_k-1} e^{-x/\theta_k}}{\Gamma(\alpha_k) \theta_k^{\alpha_k}}$ , where  $\alpha_k = \frac{(P-K+1+(K-1)\hat{\rho}_k)^2}{P-K+1+(K-1)\delta_k}$  and  $\theta_k$  is given by (3-27). By applying this approximate distribution, we have

$$\mathbb{E} \left\{ \frac{1}{\gamma_k} \right\} = \frac{\Gamma(\alpha_k - 1)}{\Gamma(\alpha_k) \theta_k} = \frac{1}{(\alpha_k - 1) \theta_k}, \quad (6-22)$$

where the last equality is resulted from  $\Gamma(x + 1) = x\Gamma(x)$ . By Substituting (6-22) into (6-21), the rate given by Theorem 3 can be concluded.

It is worth mentioning that by applying the same method, an upper bound for the rate given by (6-20) can also be found as  $R_k^{LMMSE} \leq \log_2(1 + \mathbb{E}\{\gamma_k\}) = \log_2(1 + \alpha_k \theta_k)$ . This verifies that the closed-form ergodic rate given by Theorem 3 is very accurate and close to the exact ergodic rate, especially in lower values of SNR, where  $\theta_k$  is very small.

## Chapter 7: REFERENCES

- [1] R. Chataut and R. Akl, “Massive MIMO systems for 5G and beyond networks—overview, recent trends, challenges, and future research direction,” *Sensors*, vol. 20, no. 10, p. 2753, 2020.
- [2] F. B. Saghezchi *et al.*, “Drivers for 5G: The ‘Pervasive Connected World,’” *Fundam. 5G Mob. Networks*, pp. 1–27, 2015.
- [3] T. Chen, M. Matinmikko, X. Chen, X. Zhou, and P. Ahokangas, “Software defined mobile networks: concept, survey, and research directions,” *IEEE Commun. Mag.*, vol. 53, no. 11, pp. 126–133, 2015.
- [4] S. A. Busari, K. M. S. Huq, S. Mumtaz, L. Dai, and J. Rodriguez, “Millimeter-wave massive MIMO communication for future wireless systems: A survey,” *IEEE Commun. Surv. Tutorials*, vol. 20, no. 2, pp. 836–869, 2017.
- [5] D. Wu, J. Wang, Y. Cai, and M. Guizani, “Millimeter-wave multimedia communications: challenges, methodology, and applications,” *IEEE Commun. Mag.*, vol. 53, no. 1, pp. 232–238, 2015.
- [6] X. Wang *et al.*, “Millimeter wave communication: A comprehensive survey,” *IEEE Commun. Surv. Tutorials*, vol. 20, no. 3, pp. 1616–1653, 2018.
- [7] R. CHAKRABORTY, N. KUMARI, M. MOUSAM, and A. MUKHERJEE, “The future of 5G and millimeter waves,” in *2018 Second International Conference on Electronics, Communication and Aerospace Technology (ICECA)*, 2018, pp. 1679–1683.
- [8] S. Rangan, T. S. Rappaport, and E. Erkip, “Millimeter-wave cellular wireless networks: Potentials and challenges,” *Proc. IEEE*, vol. 102, no. 3, pp. 366–385, 2014.
- [9] T. L. Marzetta, “Noncooperative cellular wireless with unlimited numbers of base station antennas,” *IEEE Trans. Wirel. Commun.*, vol. 9, no. 11, pp. 3590–3600, 2010.
- [10] F. Rusek *et al.*, “Scaling up MIMO: Opportunities and challenges with very large arrays,” *arXiv Prepr. arXiv1201.3210*, 2012.
- [11] E. G. Larsson, O. Edfors, F. Tufvesson, and T. L. Marzetta, “Massive MIMO for next

- generation wireless systems,” *IEEE Commun. Mag.*, vol. 52, no. 2, pp. 186–195, 2014.
- [12] T. L. Marzetta, “Massive MIMO: an introduction,” *Bell Labs Tech. J.*, vol. 20, pp. 11–22, 2015.
- [13] Q. C. Li, H. Niu, A. T. Papathanassiou, and G. Wu, “5G network capacity: Key elements and technologies,” *IEEE Veh. Technol. Mag.*, vol. 9, no. 1, pp. 71–78, 2014.
- [14] M. Kamel, W. Hamouda, and A. Youssef, “Ultra-dense networks: A survey,” *IEEE Commun. Surv. Tutorials*, vol. 18, no. 4, pp. 2522–2545, 2016.
- [15] D. López-Pérez, M. Ding, H. Claussen, and A. H. Jafari, “Towards 1 Gbps/UE in cellular systems: Understanding ultra-dense small cell deployments,” *IEEE Commun. Surv. Tutorials*, vol. 17, no. 4, pp. 2078–2101, 2015.
- [16] Nokia, “Ultra Dense Network (UDN),” *Nokia*, p. 27, 2016, [Online]. Available: [https://onestore.nokia.com/asset/200295/Nokia\\_Ultra\\_Dense\\_Network\\_White\\_Paper\\_EN.pdf](https://onestore.nokia.com/asset/200295/Nokia_Ultra_Dense_Network_White_Paper_EN.pdf).
- [17] L. Lu, G. Y. Li, A. L. Swindlehurst, A. Ashikhmin, and R. Zhang, “An overview of massive MIMO: Benefits and challenges,” *IEEE J. Sel. Top. Signal Process.*, vol. 8, no. 5, pp. 742–758, 2014.
- [18] M. A. Albreem, M. Juntti, and S. Shahabuddin, “Massive MIMO Detection Techniques: A Survey,” *IEEE Commun. Surv. Tutorials*, 2019.
- [19] H. Q. Ngo, E. G. Larsson, and T. L. Marzetta, “Energy and spectral efficiency of very large multiuser MIMO systems,” *IEEE Trans. Commun.*, vol. 61, no. 4, pp. 1436–1449, 2013.
- [20] J. Hoydis, S. Ten Brink, and M. Debbah, “Massive MIMO in the UL/DL of cellular networks: How many antennas do we need?,” *IEEE J. Sel. Areas Commun.*, vol. 31, no. 2, pp. 160–171, 2013.
- [21] L. Liu, Y. Chi, C. Yuen, Y. L. Guan, and Y. Li, “Capacity-achieving MIMO-NOMA: iterative LMMSE detection,” *IEEE Trans. Signal Process.*, vol. 67, no. 7, pp. 1758–1773, 2019.
- [22] H. Q. Ngo, E. G. Larsson, and T. L. Marzetta, “The multicell multiuser MIMO uplink with

- very large antenna arrays and a finite-dimensional channel,” *IEEE Trans. Commun.*, vol. 61, no. 6, pp. 2350–2361, 2013.
- [23] D. Chizhik, G. J. Foschini, M. J. Gans, and R. A. Valenzuela, “Keyholes, correlations, and capacities of multielement transmit and receive antennas,” *IEEE Trans. Wirel. Commun.*, vol. 1, no. 2, pp. 361–368, 2002.
- [24] A. G. Burr, “Capacity bounds and estimates for the finite scatterers MIMO wireless channel,” *IEEE J. Sel. Areas Commun.*, pp. 812–818, 2003.
- [25] T. L. Marzetta, *Fundamentals of massive MIMO*. Cambridge University Press, 2016.
- [26] A. Chockalingam and B. S. Rajan, *Large MIMO systems*. Cambridge University Press, 2014.
- [27] A.-S. Bana *et al.*, “Massive MIMO for internet of things (IoT) connectivity,” *Phys. Commun.*, vol. 37, p. 100859, 2019.
- [28] L. You *et al.*, “Network massive MIMO transmission over millimeter-wave and terahertz bands: Mobility enhancement and blockage mitigation,” *IEEE J. Sel. Areas Commun.*, vol. 38, no. 12, pp. 2946–2960, 2020.
- [29] H. Q. Ngo, A. Ashikhmin, H. Yang, E. G. Larsson, and T. L. Marzetta, “Cell-free massive MIMO versus small cells,” *IEEE Trans. Wirel. Commun.*, vol. 16, no. 3, pp. 1834–1850, 2017.
- [30] E. Nayebi, A. Ashikhmin, T. L. Marzetta, and B. D. Rao, “Performance of cell-free massive MIMO systems with MMSE and LSFD receivers,” in *2016 50th Asilomar Conference on Signals, Systems and Computers*, 2016, pp. 203–207.
- [31] E. Nayebi, A. Ashikhmin, T. L. Marzetta, H. Yang, and B. D. Rao, “Precoding and power optimization in cell-free massive MIMO systems,” *IEEE Trans. Wirel. Commun.*, vol. 16, no. 7, pp. 4445–4459, 2017.
- [32] A. A. I. Ibrahim, A. Ashikhmin, T. L. Marzetta, and D. J. Love, “Cell-free massive MIMO systems utilizing multi-antenna access points,” in *2017 51st Asilomar Conference on Signals, Systems, and Computers*, 2017, pp. 1517–1521.

- [33] H. Q. Ngo, L.-N. Tran, T. Q. Duong, M. Matthaiou, and E. G. Larsson, “On the total energy efficiency of cell-free massive MIMO,” *IEEE Trans. Green Commun. Netw.*, vol. 2, no. 1, pp. 25–39, 2017.
- [34] S. Elhoushy and W. Hamouda, “Downlink Performance of Limited-Fronthaul Cell-Free Massive MIMO,” in *ICC 2021-IEEE International Conference on Communications*, 2021, pp. 1–6.
- [35] G. Interdonato, E. Björnson, H. Q. Ngo, P. Frenger, and E. G. Larsson, “Ubiquitous cell-free massive MIMO communications,” *EURASIP J. Wirel. Commun. Netw.*, vol. 2019, no. 1, p. 197, 2019.
- [36] H. Q. Ngo, E. G. Larsson, and T. L. Marzetta, “Aspects of favorable propagation in massive MIMO,” in *2014 22nd European Signal Processing Conference (EUSIPCO)*, 2014, pp. 76–80.
- [37] Z. Chen and E. Björnson, “Channel hardening and favorable propagation in cell-free massive MIMO with stochastic geometry,” *IEEE Trans. Commun.*, vol. 66, no. 11, pp. 5205–5219, 2018.
- [38] M. Bashar, K. Cumanan, A. G. Burr, H. Q. Ngo, and M. Debbah, “Cell-free massive MIMO with limited backhaul,” in *2018 IEEE International Conference on Communications (ICC)*, 2018, pp. 1–7.
- [39] Q. Zhang, S. Jin, K.-K. Wong, H. Zhu, and M. Matthaiou, “Power scaling of uplink massive MIMO systems with arbitrary-rank channel means,” *IEEE J. Sel. Top. Signal Process.*, vol. 8, no. 5, pp. 966–981, 2014.
- [40] T. L. Marzetta, “How much training is required for multiuser MIMO?,” in *2006 fortieth asilomar conference on signals, systems and computers*, 2006, pp. 359–363.
- [41] J. Jose, A. Ashikhmin, T. L. Marzetta, and S. Vishwanath, “Pilot contamination and precoding in multi-cell TDD systems,” *IEEE Trans. Wirel. Commun.*, vol. 10, no. 8, pp. 2640–2651, 2011.
- [42] S. M. Shahabi, M. Ardebilipour, and Y. Omid, “Low-complexity fairness-driven pilot decontamination schemes for multi-cell massive MIMO systems,” *Phys. Commun.*, vol. 36,

- p. 100803, 2019.
- [43] Y. Wang, C. Li, Y. Huang, D. Wang, T. Ban, and L. Yang, “Energy-efficient optimization for downlink massive MIMO FDD systems with transmit-side channel correlation,” *Ieee Trans. Veh. Technol.*, vol. 65, no. 9, pp. 7228–7243, 2015.
  - [44] O. Saatlou, M. O. Ahmad, and M. N. S. Swamy, “Spectral efficiency maximization of a single cell massive MU-MIMO down-link TDD system by appropriate resource allocation,” *IEEE Access*, vol. 7, pp. 182758–182771, 2019.
  - [45] H. Yang and T. L. Marzetta, “Performance of conjugate and zero-forcing beamforming in large-scale antenna systems,” *IEEE J. Sel. Areas Commun.*, vol. 31, no. 2, pp. 172–179, 2013.
  - [46] H. Q. Ngo and E. G. Larsson, “Blind estimation of effective downlink channel gains in massive MIMO,” in *2015 IEEE International Conference on Acoustics, Speech and Signal Processing (ICASSP)*, 2015, pp. 2919–2923.
  - [47] M. Wang and D. Wang, “Sum-rate of multi-user MIMO systems with multi-cell pilot contamination in correlated Rayleigh fading channel,” *Entropy*, vol. 21, no. 6, p. 573, 2019.
  - [48] F. A. Pereira de Figueiredo, D. A. Mendes Lemes, C. Ferreira Dias, and G. Fraidenraich, “Massive MIMO channel estimation considering pilot contamination and spatially correlated channels,” *Electron. Lett.*, vol. 56, no. 8, pp. 410–413, 2020.
  - [49] R. R. Muller, “A random matrix model of communication via antenna arrays,” *IEEE Trans. Inf. theory*, vol. 48, no. 9, pp. 2495–2506, 2002.
  - [50] M. Miriestahbanati and M. R. Soleymani, “Spectral Efficiency Maximization of Multiuser Massive MIMO with a Finite Dimensional Channel,” in *ICC 2019-2019 IEEE International Conference on Communications (ICC)*, 2019, pp. 1–7.
  - [51] O. Saatlou, M. O. Ahmad, and M. N. S. Swamy, “Spectral efficiency maximization of multiuser massive MIMO systems with finite-dimensional channel via control of users’ power,” *IEEE Trans. Circuits Syst. II Express Briefs*, vol. 65, no. 7, pp. 883–887, 2017.
  - [52] H. Q. Ngo, M. Matthaiou, and E. G. Larsson, “Massive MIMO with optimal power and

- training duration allocation,” *IEEE Wirel. Commun. Lett.*, vol. 3, no. 6, pp. 605–608, 2014.
- [53] A. Khansefid and H. Minn, “Asymptotically optimal power allocation for massive MIMO uplink,” in *2014 IEEE Global Conference on Signal and Information Processing (GlobalSIP)*, 2014, pp. 627–631.
- [54] Q. Zhang, S. Jin, M. McKay, D. Morales-Jimenez, and H. Zhu, “Power allocation schemes for multicell massive MIMO systems,” *IEEE Trans. Wirel. Commun.*, vol. 14, no. 11, pp. 5941–5955, 2015.
- [55] H. V. Cheng, E. Björnson, and E. G. Larsson, “Uplink pilot and data power control for single cell massive MIMO systems with MRC,” in *2015 International Symposium on Wireless Communication Systems (ISWCS)*, 2015, pp. 396–400.
- [56] H. V. Cheng, E. Björnson, and E. G. Larsson, “Optimal pilot and payload power control in single-cell massive MIMO systems,” *IEEE Trans. Signal Process.*, vol. 65, no. 9, pp. 2363–2378, 2016.
- [57] L. You, Y. Huang, D. Zhang, Z. Chang, W. Wang, and X. Gao, “Energy Efficiency Optimization for Multi-cell Massive MIMO: Centralized and Distributed Power Allocation Algorithms,” *IEEE Trans. Commun.*, 2021.
- [58] O. Saatlou, M. O. Ahmad, and M. N. S. Swamy, “Joint data and pilot power allocation for massive MU-MIMO downlink TDD systems,” *IEEE Trans. Circuits Syst. II Express Briefs*, vol. 66, no. 3, pp. 512–516, 2018.
- [59] M. Miriestahbanati, O. Saatlou, and M. R. Soleymani, “Maximizing the spectral efficiency of finite dimensional multiuser massive MIMO,” *Phys. Commun.*, p. 101430, 2021.
- [60] S. Vishwanath, N. Jindal, and A. Goldsmith, “Duality, achievable rates, and sum-rate capacity of Gaussian MIMO broadcast channels,” *IEEE Trans. Inf. theory*, vol. 49, no. 10, pp. 2658–2668, 2003.
- [61] E. Björnson, E. G. Larsson, and M. Debbah, “Massive MIMO for maximal spectral efficiency: How many users and pilots should be allocated?,” *IEEE Trans. Wirel. Commun.*, vol. 15, no. 2, pp. 1293–1308, 2015.

- [62] T. T. Do, E. Björnson, E. G. Larsson, and S. M. Razavizadeh, “Jamming-resistant receivers for the massive MIMO uplink,” *IEEE Trans. Inf. Forensics Secur.*, vol. 13, no. 1, pp. 210–223, 2017.
- [63] S. Jin, X. Wang, Z. Li, K.-K. Wong, Y. Huang, and X. Tang, “On massive MIMO zero-forcing transceiver using time-shifted pilots,” *IEEE Trans. Veh. Technol.*, vol. 65, no. 1, pp. 59–74, 2015.
- [64] Q. H. Spencer, A. L. Swindlehurst, and M. Haardt, “Zero-forcing methods for downlink spatial multiplexing in multiuser MIMO channels,” *IEEE Trans. signal Process.*, vol. 52, no. 2, pp. 461–471, 2004.
- [65] C.-B. Chae, D. Mazzarese, N. Jindal, and R. W. Heath, “Coordinated beamforming with limited feedback in the MIMO broadcast channel,” *IEEE J. Sel. Areas Commun.*, vol. 26, no. 8, pp. 1505–1515, 2008.
- [66] K. S. Gomadam, H. C. Papadopoulos, and C.-E. Sundberg, “Techniques for multi-user MIMO with two-way training,” in *2008 IEEE International Conference on Communications*, 2008, pp. 3360–3366.
- [67] S. M. Kay, *Fundamentals of statistical signal processing*. Prentice Hall PTR, 1993.
- [68] S. Boyd and L. Vandenberghe, *Convex optimization*. Cambridge university press, 2004.
- [69] T. Van Chien, T. N. Canh, E. Björnson, and E. G. Larsson, “Power control in cellular massive MIMO with varying user activity: A deep learning solution,” *IEEE Trans. Wirel. Commun.*, vol. 19, no. 9, pp. 5732–5748, 2020.
- [70] G. Interdonato, H. Q. Ngo, E. G. Larsson, and P. Frenger, “How much do downlink pilots improve cell-free massive MIMO?,” in *2016 IEEE Global Communications Conference (GLOBECOM)*, 2016, pp. 1–7.
- [71] A. M. Tulino and S. Verdú, “Random matrix theory and wireless communications,” *Found. Trends® Commun. Inf. Theory*, vol. 1, no. 1, pp. 1–182, 2004.